The KRAS-regulated kinome identifies WEE1 and ERK coinhibition as a potential therapeutic strategy in KRAS-mutant pancreatic cancer

J. Nathaniel Diehl[1], Jennifer E. Klomp[2], Kayla R. Snare[2], Priya S. Hibshman[2,3], Devon R. Blake[4], Zane D. Kaiser[2], Thomas S. K. Gilbert[3,5], Elisa Baldelli[6], Mariaelena Pierobon[6], Björn Papke[2], Runying Yang[2], Richard G. Hodge[2], Naim U. Rashid[2,7], Emanuel F. Petricoin III[6], Laura E. Herring[3,5], Lee M. Graves[2,3,5], Adrienne D. Cox[2,3,4,8], and Channing J. Der[1,2,3,4,*]

From the [1]Curriculum in Genetics and Molecular Biology, [2]Lineberger Comprehensive Cancer Center, [3]Cell Biology and Physiology Curriculum, [4]Department of Pharmacology, [5]UNC Michael Hooker Proteomics Center, University of North Carolina at Chapel Hill, Chapel Hill, North Carolina, USA; [6]Center for Applied Proteomics and Molecular Medicine, George Mason University, Manassas, Virginia, USA; [7]Department of Biostatistics and [8]Department of Radiation Oncology, University of North Carolina at Chapel Hill, Chapel Hill, North Carolina, USA

Edited by Eric Fearon

Oncogenic KRAS drives cancer growth by activating diverse signaling networks, not all of which have been fully delineated. We set out to establish a system-wide profile of the KRAS-regulated kinase signaling network (kinome) in KRAS-mutant pancreatic ductal adenocarcinoma (PDAC). We knocked down KRAS expression in a panel of six cell lines and then applied multiplexed inhibitor bead/MS to monitor changes in kinase activity and/or expression. We hypothesized that depletion of KRAS would result in downregulation of kinases required for KRAS-mediated transformation and in upregulation of other kinases that could potentially compensate for the deleterious consequences of the loss of KRAS. We identified 15 upregulated and 13 downregulated kinases in common across the panel of cell lines. In agreement with our hypothesis, all 15 of the upregulated kinases have established roles as cancer drivers (e.g., SRC, TGF-β1, ILK), and pharmacological inhibition of one of these upregulated kinases, DDR1, suppressed PDAC growth. Interestingly, 11 of the 13 downregulated kinases have established driver roles in cell cycle progression, particularly in mitosis (e.g., WEE1, Aurora A, PLK1). Consistent with a crucial role for the downregulated kinases in promoting KRAS-driven proliferation, we found that pharmacological inhibition of WEE1 also suppressed PDAC growth. The unexpected paradoxical activation of ERK upon WEE1 inhibition led us to inhibit both WEE1 and ERK concurrently, which caused further potent growth suppression and enhanced apoptotic death compared with WEE1 inhibition alone. We conclude that system-wide delineation of the KRAS-regulated kinome can identify potential therapeutic targets for KRAS-mutant pancreatic cancer.

Pancreatic ductal adenocarcinoma (PDAC) is among the deadliest cancers, with a 5-year survival rate of 10% (1). Despite significant advances in our understanding of the genetic and molecular drivers of PDAC (2), effective targeted therapies are still lacking. Current standards of care are comprised of conventional cytotoxic drugs (3).

Mutational activation of the *KRAS* oncogene is the initiating genetic event and is found in 95% of PDACs (4). There is now substantial experimental evidence that KRAS is essential for the maintenance of PDAC growth, and consequently, the National Cancer Institute has identified the development of anti-KRAS therapeutic strategies as one of the four major initiatives in the field (https://deainfo.nci.nih.gov/advisory/ctac/archive/0313/PCwgReport.pdf). Recent early stage clinical findings with direct inhibitors of one KRAS mutant, G12C, support the potential clinical impact of an effective KRAS inhibitor (5, 6). However, while KRAS^{G12C} mutations are common in lung adenocarcinoma, they comprise only 2% of *KRAS* mutations in PDAC (4, 7). Therefore, indirect strategies to block aberrant KRAS signaling remain arguably the best approach for the majority of KRAS-mutant PDAC (8).

One key approach is to inhibit downstream effector signaling. Of the multitude of KRAS effectors, at least four are validated drivers of KRAS-dependent PDAC growth (7). The best characterized and potentially most crucial is the RAF–mitogen-activated protein kinase/extracellular signal–regulated kinase (ERK) kinase (MEK)–ERK mitogen-activated protein kinase (MAPK) cascade. That activated *Braf* can phenocopy mutant *Kras* and, together with *Tp53* mutations, drive full development of metastatic PDAC in mouse models, which supports the key role of the MAPK cascade in driving Kras-dependent PDAC growth (9). While the substrates of RAF and MEK kinases are highly restricted, ERK1/2 serine/threonine kinase activation can cause direct or indirect phosphorylation of a diverse spectrum of more than one thousand proteins (10). Since ERK substrates include other protein kinases (e.g., ribosomal S6 kinases 1–4, MAPK-interacting kinase 2, and mitogen- and stress-activated kinases 1/2), ERK activation can regulate a highly diverse

phosphoproteome (11). However, the specific components are context dependent, and the ERK-regulated phosphoproteome downstream of KRAS in PDAC is not well delineated.

The second best characterized KRAS effectors are PI3Ks (12). KRAS activation of PI3K promotes formation of phosphatidylinositol-(3−5)-triphosphate, leading to activation of the AKT and mammalian target of rapamycin (mTOR) serine/threonine kinases. Activation of PI3K−AKT−mTOR signaling has also been observed as a compensatory response to ERK inhibition, driving resistance to ERK MAPK inhibitors (13, 14). Thus, concurrent PI3K inhibition synergistically enhances the antitumor activity of ERK MAPK inhibitors (9). Other key KRAS effectors include the RAL (RAS like) and RAC small GTPases, which activate TANK-binding kinase 1 and p21-activated kinase serine/threonine kinases (7). With their high tractability as therapeutic targets, these and other protein kinase components of KRAS effector signaling have been pursued as indirect approaches to KRAS inhibition (15). We propose that still other kinases may also be of interest as targets in KRAS-mutant PDAC.

In addition, a limitation of essentially all targeted anticancer therapies is the onset of treatment-induced acquired resistance (16, 17). In response to pharmacological inhibition of a key cancer driver, cancer cells can induce a complex array of responses that functionally compensate for target inhibition. One major mechanism of resistance is loss of the negative feedback signaling that tempers the strength of growth regulatory signaling networks (18). For example, although aberrant ERK activation can drive cancer growth, excessive ERK activity is deleterious, causing growth cessation through induction of senescence or apoptosis (19−21). Therefore, a multitude of ERK-dependent negative feedback loops exist to dampen ERK activity (22). Thus, upon pharmacological inhibition of ERK, loss of ERK-dependent negative feedback leads to ERK reactivation to overcome inhibitor action. Similar responses are also seen upon inhibition of the PI3K−AKT−mTOR pathway (23).

An important strategy to improve the long-term efficacy of targeted therapies is the elucidation of treatment-induced resistance mechanisms, which can then be used to identify drug combinations capable of blocking or even reversing the onset of resistance. Unbiased system-wide screening methods applied for this purpose include powerful genetic approaches such as CRISPR- or RNAi-mediated loss of function or complementary DNA (cDNA) overexpression/activation gain-of-function screens (24). For example, a CRISPR−Cas9 screen demonstrated that ERK reactivation is a primary mechanism limiting the efficacy of KRAS[G12C] inhibitors (25). These findings have guided initiation of ongoing clinical trials to evaluate KRAS[G12C] inhibitors in combination with inhibitors that act either upstream (*e.g.,* on epidermal growth factor receptor [EGFR], SH2 domain−containing phosphatase-2 [SHP2], SOS1 [SOS Ras/Rac guanine nucleotide exchange factor 1]) or downstream (*e.g.,* on MEK) of KRAS (NCT03600883, NCT04185883, and NCT04330664). Similarly, Wood *et al.* (24) applied an activated signaling expression library to identify both known and novel mechanisms that drive resistance to ERK MAPK inhibitors (26). In a complementary approach, our

chemical library screen demonstrated that concurrent inhibition of other ERK MAPK components, to block compensatory ERK reactivation, synergistically enhanced the efficacy of RAF inhibitors in KRAS-mutant PDAC (27).

In light of the key role of kinome reprogramming in driving resistance, it is crucial to be able to detect changes in kinase activity and/or expression in response to pharmacological inhibition of an oncogenic signaling driver. Chemical proteomics is a particularly powerful experimental technique that enables kinome-wide profiling of these changes. One version of this type of assay, multiplexed inhibitor bead (MIB)/MS, incorporates MIBs, coupled to MS (28). MIBs, comprised of broad-spectrum kinase inhibitors covalently coupled to Sepharose beads, can be used to monitor protein kinase expression and/or activation, where MIB-associated kinases are identified by MS. In our initial application of MIB/MS, we identified activation of multiple receptor tyrosine kinases (RTKs) in response to MEK inhibitor (MEKi) treatment that may drive MEKi resistance in KRAS-mutant breast cancer (29). Accordingly, concurrent inhibition of RTKs and MEK more effectively impaired transformed and tumor growth *in vitro* and *in vivo* than MEKi alone. We have also applied MIB/MS to identify novel inhibitors of chemotherapy-resistant PDAC (30), pinpoint tumor cell type−specific responses to the clinical kinase inhibitor dasatinib in diffuse large B-cell lymphoma (31), and identify EGFR/human epidermal growth factor receptor 2 activation of the MEK5−ERK5 MAPK cascade as compensatory response to ERK1/2 inhibition, which drives resistance to ERK inhibitor (ERKi) treatment by stabilizing the MYC oncoprotein (32).

In the present study, we hypothesized that a system-wide delineation of KRAS-regulated kinases can identify therapeutic targets that may not have been considered based on our current knowledge of KRAS effector signaling networks. We speculated that KRAS may require additional kinases beyond the classical RAF−MEK−ERK and PI3K−AKT−mTOR effector pathways to promote its transforming functions, and that these would be downregulated upon KRAS depletion. In contrast, we anticipated that yet other kinases would be upregulated as compensatory responses to this depletion. Thus, identification of both upregulated as well as downregulated kinases may establish novel targets for anti-KRAS therapies. We therefore applied the kinome-wide MIB/MS assay to elucidate an unbiased profile of the KRAS-dependent kinome in PDAC. Our strategy further elucidates the complex spectrum of protein kinases functionally linked to aberrant KRAS activation and identifies unanticipated signaling vulnerabilities and potential therapeutic approaches for PDAC.

Results

KRAS suppression alters the activity of diverse kinases in PDAC

Although oncogenic KRAS effector signaling activates the ERK MAPK cascade and other protein kinases, we speculated that the full spectrum of KRAS-regulated protein kinases remained to be elucidated. To gain a full understanding of the KRAS-dependent kinome in KRAS-mutant PDAC, we

suppressed *KRAS* expression in a panel of six KRAS-mutant PDAC cell lines using validated siRNA (Fig. S1*A*). Although all cell lines harbor mutant *KRAS* and show KRAS-dependent growth (13), nevertheless, they exhibit significant genetic heterogeneity (Table S1). Aside from the four major genetic alterations found in PDAC, the majority of genetic alterations are found at single digit frequencies (33–37).

After 72 h, a time point at which compensatory changes in the kinome have been initiated in response to loss of KRAS (27), cell lysates were processed for MIB/MS label-free proteomics to monitor kinome-wide changes in activity and/or expression (Fig. S1*B* and Data Files S1–S3). Our approach detected a total of 227 kinases of sufficient abundance for quantification in one or more PDAC cell lines (Fig. S1*C*). As expected, given the genetic heterogeneity of PDAC tumors, there was significant heterogeneity in the kinase profile of each cell line (Fig. S1*C*). Interestingly, the quantified kinases were upregulated and downregulated to the same degree (63 and 62 kinases, respectively; Fig. S1*D*). Across all six lines, we identified 15 kinases that were significantly upregulated and 13 that were downregulated in common (Figs. 1*A* and S1*E*).

To determine if the deregulated kinases represented specific subgroups, we applied the UniProt kinase classification annotation that is based in part on catalytic domain sequence identity and in part on biological function (Fig. S1*F*). Notably, although the downregulated kinases did not share much sequence identity (7/13 or 53.8% were "other" kinases *versus* 32/227 or 14.1% of all detected kinases) (Fig. S1, *F* and *G*), nearly all have established roles in regulating cell cycle transitions, particularly through mitosis (*e.g.*, Aurora kinase A [*AURKA*], CHK1 [*CHEK1*], WEE1) (Table S2).

In contrast, the upregulated kinases were enriched in tyrosine kinases and tyrosine kinase–like kinases (7/15; 46.7%), which comprised 23.3% (53/227) of all detected kinases (Fig. S1, *F* and *H*). Strikingly, a driver role in cancer has been attributed to all 15 upregulated kinases (*e.g.*, ERK1 [*MAPK3*] [Table S3], SRC, and Janus kinase [JAK]), supporting the strong likelihood that upregulated kinases serve compensatory growth-promoting roles that attenuate the deleterious consequences of KRAS deficiency. Supporting this possibility, we showed recently that ERKi treatment of PDAC cell lines caused upregulation of SRC activity and that concurrent SRC inhibition further enhanced ERKi–mediated growth suppression (32).

To complement these kinome analyses, we used reverse phase protein array (RPPA) pathway activation mapping (38) to evaluate the signaling consequences of 72 h of siRNA-mediated *KRAS* suppression (Fig. S1*I*). The RPPA panel included 149 phospho-specific and total antibodies to monitor the activation state or expression, respectively, of signaling proteins involved in regulation of cell proliferation, survival, motility, and others (Table S4 and Data File S4). One caution regarding RPPA analyses is the limited repertoire of validated antibodies included in the analyses. Since only antibodies that recognize a single band by Western blot analyses of total cellular proteins can be used, our analyses did not include antibodies that monitored signaling with some of our identified KRAS-dependent kinases.

As expected, phosphorylated and total ERK proteins were increased, consistent with loss of ERK-dependent negative feedback signaling (Fig. S1*J*). Nevertheless, phosphorylation of key ERK substrates important for driving ERK-dependent growth (ribosomal S6 kinase, ELK1, and MYC) remained strongly suppressed (Fig. S1*J*). Thus, similar to our previous observations with pharmacological inhibition of ERK (13, 14), the level of ERK phosphorylation did not reliably reflect the level of ERK signaling.

Among the decreases in expression and/or activation of multiple proteins involved in cell cycle regulation were a dramatic reduction in the mitotic marker, phosphorylated histone H3 at Ser^{10}, as well as loss of the proliferation markers Ki67 and phosphorylation of retinoblastoma protein at Ser^{780} (Fig. S1*I*). RPPA analyses also revealed alterations in expression (*e.g.*, Bcl-2-like protein 11, BIM) or phosphorylation (*e.g.*, FAS-associated death domain protein, FADD Ser^{194}) of proteins associated with apoptosis, a well-described consequence of loss of mutant KRAS function (39). Finally, reductions were also detected in phosphorylated S6 ribosomal protein, involved in regulation of protein translation (Fig. S1, *I* and *J*). Thus, KRAS loss is associated with the activation and inactivation of diverse growth regulatory signaling pathways.

We next wanted to determine the contribution of the ERK MAPK effector pathway to the regulation of the KRAS-dependent kinome. We treated the same panel of six PDAC cell lines for 24 h with the ERK1/2-selective inhibitor SCH772984 (ERKi) (40), then performed MIB/MS analyses (Data Files S5 and S6). Quantification of kinases revealed that, of 264 kinases detected, 26 were significantly altered in expression and/or activity across all six cell lines (Figs. 1*B* and S1*K*). Of these, seven were upregulated and 19 were downregulated. As expected, ERK1 and ERK2 (*MAPK3* and *MAPK1*) activities were by far the most strongly downregulated upon ERKi treatment (Fig. 1*B*).

Importantly, many of the same kinases were altered upon pharmacological inhibition of ERK and upon genetic suppression of KRAS. Nine of the kinases downregulated by siKRAS (Fig. 1*A*) were also downregulated by ERKi (Fig. 1*B*), including many involved in progression through mitosis. Similarly, discoidin domain receptor 1 (DDR1), JAK1, and SRC were among kinases upregulated by both siKRAS and ERKi. Spearman's rank correlation analysis of siKRAS- and ERKi-mediated kinome changes revealed significant overlap between the 222 kinases detected in both datasets (rho = 0.434; p = 1.77e-11) (Fig. 1*C*). The significant overlap in kinase signaling changes following either ERK inhibition or KRAS suppression is consistent with the predominant role of ERK MAPK in supporting KRAS-dependent PDAC growth (9, 13). We conclude that the observed kinome changes conferred by genetic suppression of KRAS were mediated in large part through loss of ERK1/2 signaling.

Inhibition of DDR1, but not JAK, impairs PDAC growth

We speculated that upregulated kinases, in particular those with known driver roles in cancer, may represent compensatory activities in response to loss of KRAS. Among the kinases upregulated following KRAS knockdown, JAK1 was notable
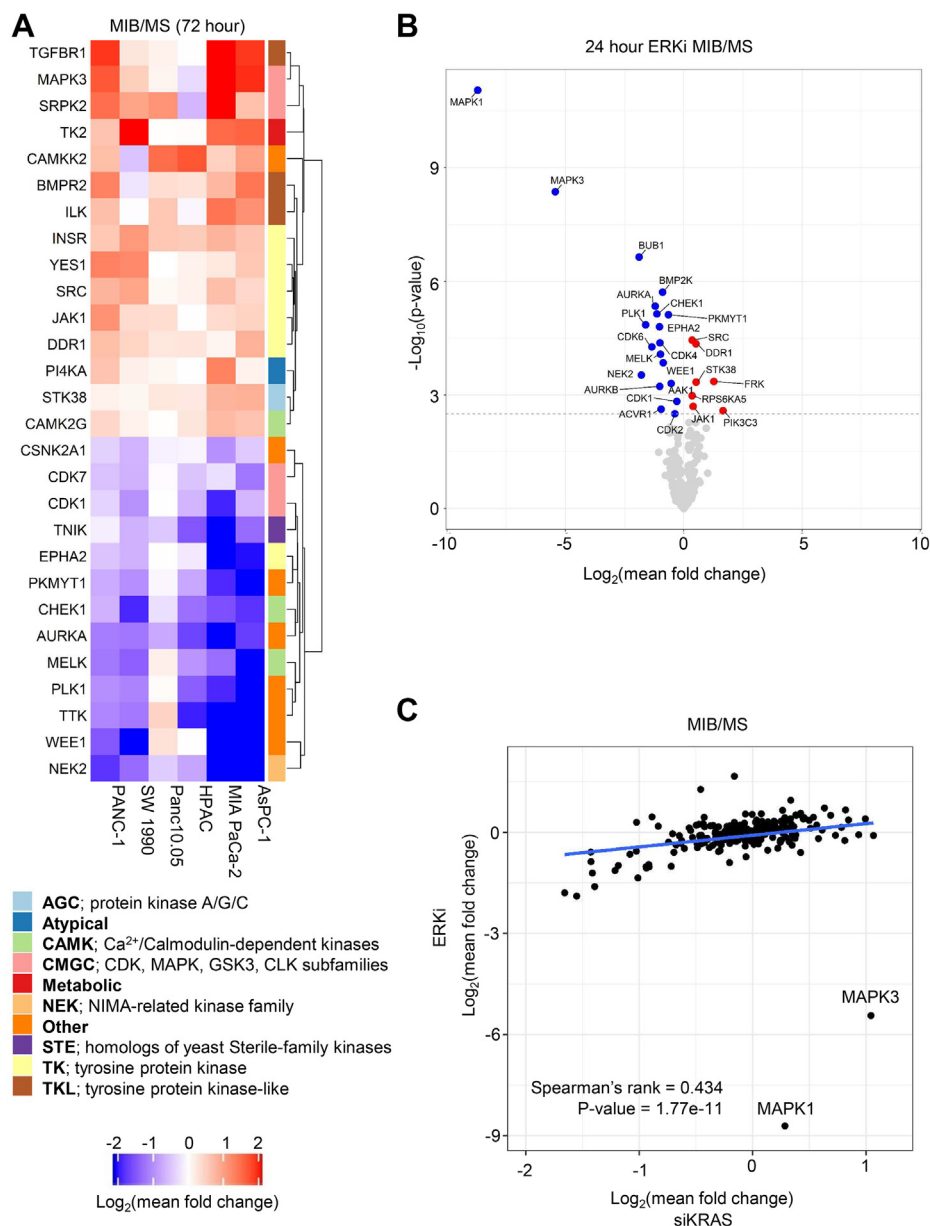
Figure 1. KRAS knockdown induces kinome-wide alterations primarily through ERK. *A,* heatmap summarizing kinases that were significantly altered (adjusted-*p* value <0.05) after 72 h of nonspecific control siRNA (siNS) or siKRAS treatment, followed by MIB/MS enrichment. Lysates were collected from six KRAS-mutant PDAC cell lines (SW 1990, MIA PaCa-2, PANC-1, HPAC, AsPC-1, and Panc 10.05). Unsupervised clustering was used to visualize distance metrics of log-transformed fold change values for significant kinases following ANOVA. Kinase class annotations were added from UniProt classification and index of kinases. *B,* volcano plot showing results of significance testing after ANOVA (*y*-axis) with the log-transformed mean fold change in ERKi (SCH772984) over DMSO control (24 h). Significant kinases are colored *red* (increased) or *blue* (decreased) if *p* value is significant (adjusted-*p* value <0.05) following Benjamini–Hochberg correction (n = 3). *C,* Spearman's rank correlation analysis of siKRAS/siNS samples *versus* ERKi/DMSO samples, 222 kinases were shared among dataset. DMSO, dimethyl sulfoxide; ERK, extracellular signal–regulated kinase; ERKi, ERK inhibitor; MIB, multiplexed inhibitor bead; PDAC, pancreatic ductal adenocarcinoma.

because the JAK1– signal transducer and activator of transcription 3 (STAT3) signaling axis has been shown to be important for PDAC tumorigenesis and can drive resistance to inhibition of MEK (41, 42). Consistent with MIB/MS, RPPA also showed that four of five cell lines displayed significant (adjusted-*p* value <0.05) activation of STAT3 following KRAS knockdown (Fig. 2A), as indicated by phosphorylation at the JAK family site Tyr[705] (43). Phosphorylation of STAT3 at Ser[727], which is not a JAK site but a possible ERK or c-Jun N-terminal kinase target (44), also increased in a cell line–

dependent manner (44), as did phosphorylation of STAT1 and STAT5. STAT6 phosphorylation at Tyr[641] was the most consistent of all, in agreement with our previous finding of significant upregulation of JAK signaling through this site upon blockade of the MAPK cascade (27). To determine whether JAK1–STAT3 was similarly affected, we directly inhibited signaling through ERK MAPK. In the presence of the ERK1/2 inhibitor SCH772984, STAT3 phosphorylation (Tyr[705]) was increased in Pa02C and Pa16C and unchanged in MIA PaCa-2 and PANC-1 cells (Fig. 2B). We conclude that
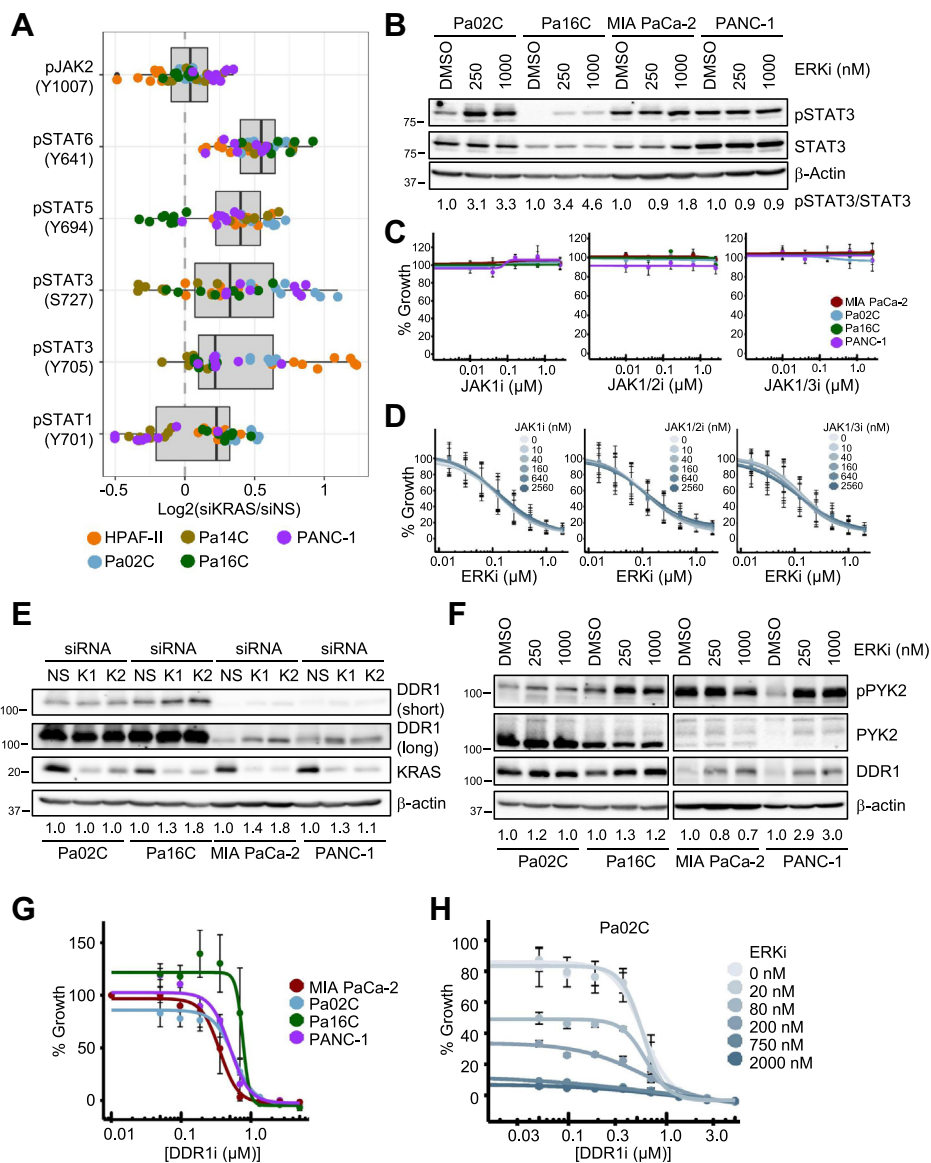
Figure 2. DDR1, but not JAK, is a therapeutic vulnerability in PDAC. *A*, reverse phase protein array of five PDAC cell lines following 72 h siRNA knockdown of KRAS. Values are log₂-transformed fold change with respect to median siNS value (n = 4). *B*, immunoblot of PDAC cell lines following treatment with vehicle or ERKi (SCH772984) for 24 h (n = 4). Ratios of pSTAT3/STAT3 are reported below the blot. *C*, proliferation of PDAC cells (5 days) following treatment with JAK1i (filgotinib), JAK1/2i (ruxolitinib), or JAK1/3i (tofacitinib) at various concentrations. Cell numbers at endpoint were normalized to vehicle-treated control (100% growth) for each cell line. Curves were fit using a 4-parameter log-logistic function and the drm package in R (n = 3). *D*, proliferation of Pa02C cells (5 days) following combination treatment with JAK1i, JAK1/2i, or JAK1/3i and ERKi (SCH772984) at various concentrations. Cell numbers were normalized, and curves were fit as in panel *C* (n = 3). *E*, immunoblot of PDAC cell lines following treatment with nonspecific (NS) or KRAS-targeting (K1 and K2) siRNA constructs for 72 h. Relative DDR1 levels are indicated below the blot (total DDR1 normalized for loading differences as determined by β-actin). "Short" and "long" indicate shorter and longer exposures of the same membrane, respectively (n = 3). *F*, immunoblot of PDAC cell lines following treatment with vehicle or ERKi (SCH772984) for 24 h (n = 4). Relative pPYK2 levels (*versus* DMSO) in each cell line are indicated below the blot. *G*, proliferation of PDAC cells (5 days) following treatment with DDR1i (7rh) at various concentrations. Cell numbers were normalized, and curves were fit as in panel *C* (n = 3). *H*, proliferation of Pa02C cells (5 days) following combination treatment with DDR1i (7rh) and ERKi (SCH772984) at various concentrations. Cell numbers were normalized, and curves were fit as in panel *C* (n = 3). Molecular weight markers are noted next to all immunoblots. DDR1, discoidin domain receptor 1; DMSO, dimethyl sulfoxide; ERKi, extracellular signal–regulated kinase inhibitor; JAK, Janus kinase; PDAC, pancreatic ductal adenocarcinoma; STAT3, signal transducer and activator of transcription 3.

upregulation of JAK1–STAT signaling induced by KRAS suppression was mediated through loss of ERK effector signaling.

We next determined if upregulation of JAK signaling is a compensatory response that can offset the growth suppression induced by loss of KRAS or ERK. We utilized three different JAK inhibitors, targeting JAK1 (filgotinib), JAK1/2 (ruxolitinib), and JAK1/3 (tofacitinib) (45). All three JAK inhibitors

reduced STAT3 phosphorylation in a dose-dependent manner, though PANC-1 cells were resistant to filgotinib (Fig. S2*A*). JAK inhibitors alone had no effect on anchorage-dependent proliferation of four PDAC cell lines (Fig. 2*C*), indicating the lack of dependence on JAK when KRAS is present. Furthermore, cotreatment of four PDAC cell lines with each JAK inhibitor in combination with ERKi revealed that concurrent JAK inhibition did not further enhance ERKi-mediated growth

suppression (Figs. 2*D* and S2*B*). Thus, while JAK activity was increased upon loss of KRAS, subsequent inhibition of JAK family kinases did not potentiate the antiproliferative effect of direct ERK inhibition in PDAC.

To further investigate whether upregulated kinases could compensate for the loss of KRAS, we next evaluated the DDR1. DDR1 is an RTK that transduces collagen-mediated proliferative signaling from stroma-associated extracellular matrix (46), and pharmacological inhibition of DDR1 function impaired PDAC growth *in vivo* in a mouse model (47, 48). Given our identification of DDR1 as a kinase that was upregulated upon KRAS suppression in PDAC cell lines *in vitro* (Fig. 1*A*), we sought to determine whether upregulated DDR1 could also serve as an increased proproliferative signal in a KRAS-dependent and tumor cell–intrinsic manner. We first determined that both KRAS knockdown and ERK inhibition increased DDR1 protein levels (Fig. 2, *E* and *F*, respectively). In addition, ERK inhibition increased phosphorylation of the DDR1 effector PYK2 (pPYK2; Fig. 2*F*) at the DDR1 phosphorylation site, Tyr^{402} (48), in three of four cell lines. Thus, we confirmed that DDR1 signaling is responsive to KRAS–ERK signaling.

To evaluate the possibility that DDR1 upregulation is a compensatory response to the growth suppression mediated by loss of KRAS–ERK, we first determined if inhibition of DDR1 alone is deleterious to growth. We treated PDAC cells with 7rh, a potent and selective ATP-competitive DDR1 inhibitor (49), and observed comparable IC_{50} (suppression of PYK2 Tyr^{402}) and GI_{50} values, supporting on-target growth inhibition (Figs. 2*G* and S2, *C* and *D*) (49). We found that concurrent inhibition of DDR1 and ERK caused dose-dependent loss of cell viability (Figs. 2*H* and S2*E*), ranging between additivity and synergy, according to BLISS analysis (Fig. S2*F*). Overall, our evaluation of kinases upregulated by siKRAS or ERKi has revealed a novel compensatory mechanism in DDR1 and a surprising dispensability of JAK signaling for PDAC anchorage-dependent cell growth and viability.

Loss of KRAS or MAPK signaling causes loss of G2/M and DNA-damage response kinases

In order to better understand the relationships among downregulated kinases following KRAS genetic suppression, we performed STRING analysis on significantly altered kinases (Fig. 3*A*). About 11 of the 13 downregulated kinases formed a tight interaction node, with only ephrin type-A receptor 2 and TRAF and NCIK-interacting protein kinase involved in distinctly separate signaling networks. Next, we utilized Panther Gene Ontology to determine the relevant biological processes (Fig. 3*B*). Given that our queried genes exclusively encode protein kinases, it was expected that "protein phosphorylation" was the top gene set identified. In addition, a main function of KRAS signaling through the ERK cascade is to promote cell cycle progression through G1 by transcriptional stimulation of *CCND1* (encoding cyclin D1), leading to CDK4/6-dependent phosphorylation and inactivation of the retinoblastoma protein tumor suppressor (50). Thus, it was

unexpected that we observed that multiple downregulated kinases are involved in G2/M checkpoint and mitotic functions (Table S1). Consistent with KRAS promotion of G1/S cell cycle progression, flow cytometry analyses in four PDAC cell lines showed that KRAS knockdown caused an increase (14–24%) in cells in G1 and a corresponding decrease (15–22%) in cells in S, albeit no significant change in the G2/M cell population (Fig. S3, *A* and *B*).

Interestingly, the 13 downregulated kinases identified in the chemical proteomics screen were also enriched for roles in DNA damage checkpoints and maintaining DNA integrity (Fig. 3*B*). We therefore queried our RPPA data for genes related to both DNA-damage repair and cell cycle, which revealed a mixed response to KRAS knockdown (Fig. S3*C*). Cyclin D1 levels were reduced, whereas cyclin A levels either increased or remained unchanged. In addition, phosphorylation of ATM at Ser^{1981} increased, whereas phosphorylation of ATR at Ser^{428} was diminished in all cell lines. Taken together, these changes suggest that loss of KRAS causes a loss of specific cell cycle–promoting factors. In addition, the changes in ATM and ATR phosphorylation, though divergent, suggest that KRAS knockdown may induce genomic stress that could also contribute to cell cycle factor changes.

While significant literature points to the importance of KRAS and ERK in promoting G1 progression, fewer studies outline the role of mutant KRAS in maintaining DNA damage checkpoint kinases, such as WEE1, PKMYT1, and CHEK1 (Fig. 3*A*) (51–53). We confirmed that KRAS knockdown caused loss of WEE1, CHEK1, and polo-like kinase 1 (PLK1) proteins (Fig. 3*C*). We also verified our MIB/MS analyses with ERKi (Fig. 1*B*), and we determined by Western blot analyses that ERKi treatment also caused a reduction in WEE1 protein and phosphorylation of the WEE1 substrate, CDK1 (Tyr15; pCDK1) (Fig. 3*D*). A recent transcriptome analysis of PDAC identified WEE1 as a potential therapeutic target (54). Therefore, we focused our further investigations on this DNA-damage checkpoint kinase.

To address a basis for the loss of WEE1 protein caused by KRAS suppression, we first examined WEE1 protein stability. Treatment with the proteasome inhibitor MG132 prevented WEE1 degradation more robustly in KRAS-suppressed samples as compared with control samples. This suggests that the absence of KRAS signaling destabilizes WEE1 protein (Figs. 3, *E* and *F* and S3, *D* and *E*). We hypothesized that KRAS, through its extensive transcriptional network, may also regulate *WEE1* transcription. Indeed, RT–PCR analyses demonstrated that loss of KRAS decreased WEE1 transcripts in all five cell lines tested (Fig. 3*G*). We conclude that WEE1 protein stability and transcription are both reduced upon KRAS suppression.

Inhibition of WEE1 kinase induces growth arrest and apoptosis in PDAC cells

The loss of WEE1 observed upon KRAS knockdown–induced growth suppression suggests that WEE1 activity may contribute to KRAS-mutant PDAC proliferation and
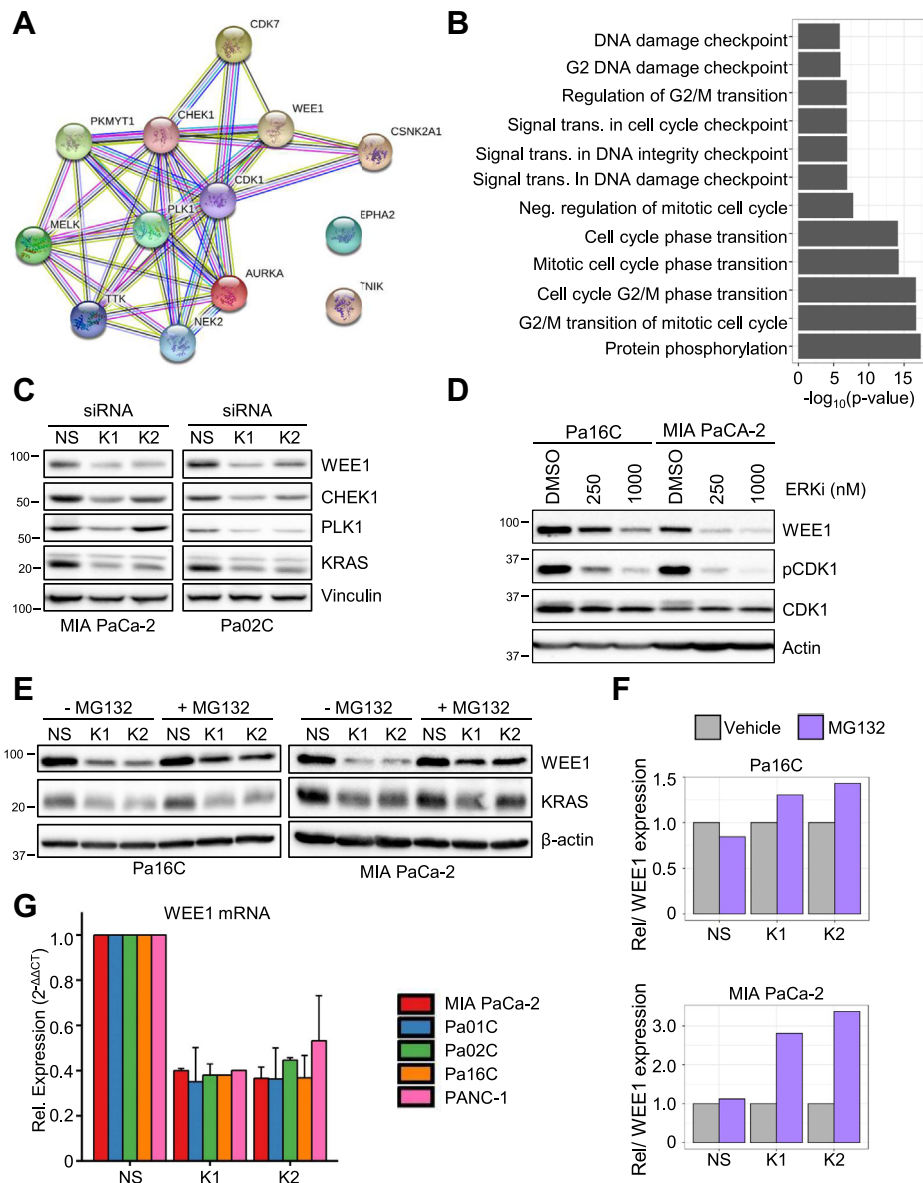
Figure 3. Loss of KRAS/MAPK signaling contributes to loss of G2/M and DNA-damage response kinases. *A*, downregulated kinase identifiers from the MIB–MS screen (Fig. 1*A*) were used as input into the STRING database, and the resulting bitmap was downloaded. Edges (lines between nodes) represent known or predicted protein–protein associations. *B*, downregulated kinase identifiers were used as input for Gene Ontology enrichment analysis of biological processes (76, 77). Selected enriched gene sets (adjusted-*p* value <0.05) are displayed along the *y*-axis, with the $-\log_{10}$-transformed *p* values displayed along the *x*-axis. *C*, immunoblot analysis of PDAC cell lines following treatment with nonspecific (NS) or KRAS-targeted (K1 and K2) siRNA constructs for 72 h (n = 4). *D*, immunoblot of PDAC cell lines following treatment with vehicle or ERKi (SCH772984) for 24 h (n = 4). *E*, protein stability of WEE1 as determined by 4 h MG132 proteasomal inhibitor treatment following 26 h treatment with NS or KRAS-targeted (K1 and K2) siRNA constructs (n = 3). *F*, quantification of blot in panel *D*. Densitometry estimates were first normalized for loading efficiency using β-actin. Next, each sample value was calculated as a ratio of MG132+/MG132− and paired by siRNA construct. *G*, quantitative RT–PCR was performed on five PDAC cell lines following 72 h treatment with NS or KRAS-targeted (K1 and K2) siRNA. Relative expression (*y*-axis) of WEE1 transcripts was measured (n = 3). Molecular weight markers are noted next to all immunoblots. ERKi, extracellular signal–regulated kinase inhibitor; MAPK, mitogen-activated protein kinase; MIB, multiplexed inhibitor bead; PDAC, pancreatic ductal adenocarcinoma.

therefore that direct inhibition of WEE1 may suppress KRAS-mediated cell proliferation. To address this possibility, we first treated cells with siRNA targeting *WEE1* and verified that loss of phosphorylation of the WEE1 substrate, CDK1 (Tyr[15]; pCDK1) was a reliable biomarker for loss of WEE1 function in PDAC (Fig. 4*A*). Similarly, treatment with the WEE1-selective clinical candidate inhibitor adavosertib/AZD1775 (WEE1i) dose-dependently reduced CDK1, with >80% reduction at 100 nM (Figs. 4*B* and S4*A*). In addition, WEE1i treatment

inhibited the proliferation of all six PDAC cell lines evaluated, with GI_{50} values (38–168 nM) comparable to the IC_{50} values (<100 nM), supporting on-target growth suppression (Figs. 4*C* and S4, *A–C*). Similar growth inhibitory activities of WEE1i were also seen in clonogenic colony formation assays (Fig. 4*D*). Consistent with previous studies (55), we found that pharmacological inhibition of WEE1 led to accumulation in S and G2/M phases of the cell cycle (Figs. 4*E*, and S4, *D* and *E*). In addition, WEE1i caused an approximately 5-fold increase in
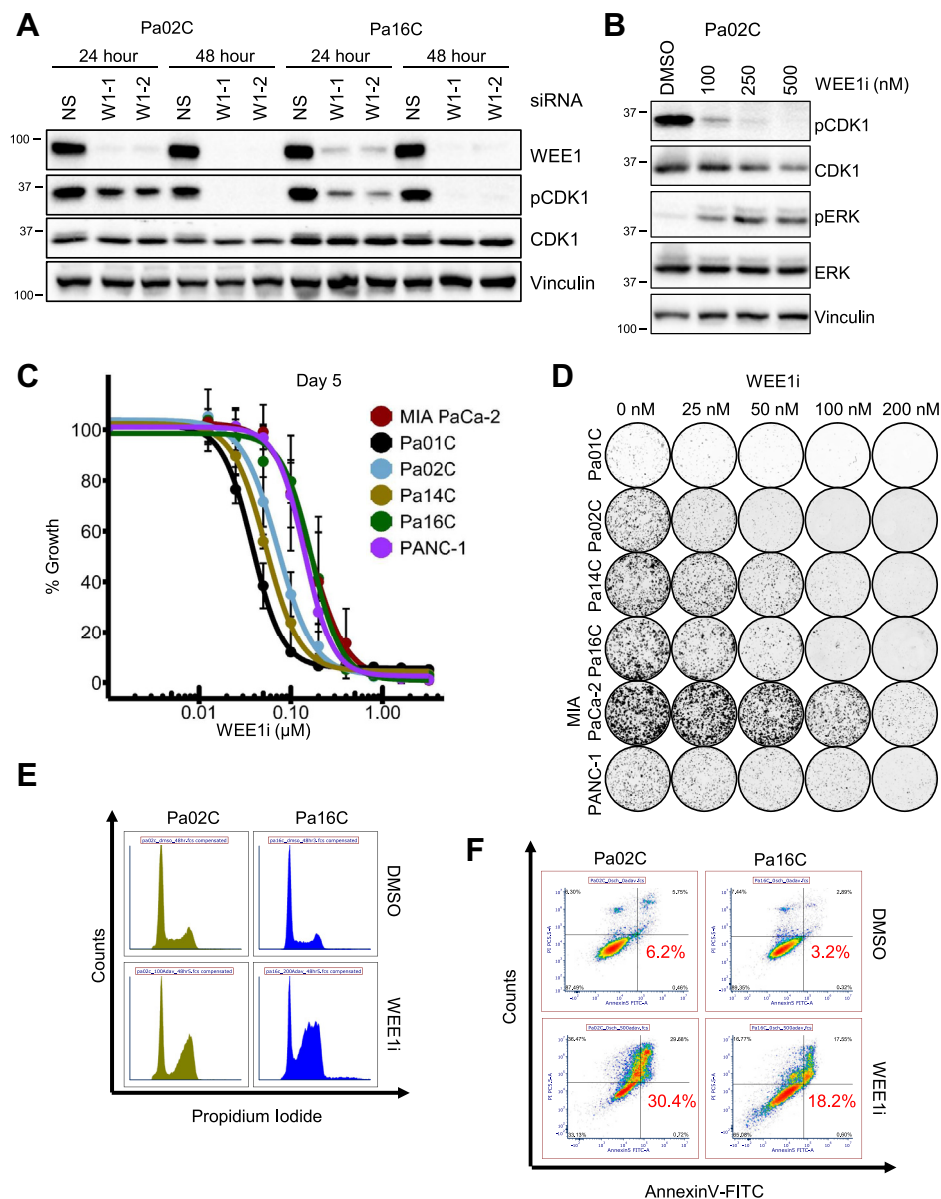
Figure 4. Inhibition of WEE1 kinase induces growth arrest and apoptosis in PDAC cells. *A*, immunoblot analysis of PDAC cell lines following treatment with nonspecific (NS) or WEE1-targeting (W1-1 and W1-2) siRNA for 24 or 48 h (n = 3). *B*, immunoblot analysis of Pa02C cells following treatment with WEE1i for 48 h (n = 4). *C*, proliferation of PDAC cells following treatment for 5 days with WEE1i (adavosertib) at various concentrations. Cell numbers at endpoint were normalized to vehicle-treated control (100% growth) for each cell line. Curves were fit using a 4-parameter log-logistic function and the drm package in R (n = 3). *D*, PDAC cells were plated at low density to allow for clonogenic growth, and various concentrations of WEE1i were added. After 10 days, plates were stained with crystal violet, and colonies were imaged (n = 4). *E*, cells were treated with vehicle or adavosertib (100 nM for Pa02C and 200 nM for Pa16C) for 24 h, then fixed, and stained with propidium iodide. Flow cytometry quantification of cell cycle populations is shown for two representative cell lines (n = 3). *F*, annexin V–FITC staining followed by flow cytometry in PDAC cell lines after 72 h treatment with 500 nM WEE1i (n = 4). Molecular weight markers are noted next to all immunoblots. PDAC, pancreatic ductal adenocarcinoma.

apoptotic cells (Fig. 4*F*). Taken together, these results support our conclusion that downregulation of WEE1 contributes to the growth suppression induced by loss of KRAS.

Combined inhibition of WEE1 and ERK causes synergistic growth arrest and apoptosis

Paradoxical activation of ERK has been reported previously in response to pharmacological inhibition of CHK1 (56, 57), another protein kinase involved in checkpoint inhibition in response to DNA damage. To determine if there is a similar response to WEE1 inhibition, we examined pERK in PDAC cell lines treated with adavosertib for 48 h. We observed a dose-dependent increase in pERK in all treated lines (Figs. 4*B* and S4, *A* and *F*). Evaluation at shorter time points showed that WEE1 activity (pCDK1) was rapidly suppressed after 6 to 24 h, whereas increased pERK was seen only after 48 h (Fig. S4*C*). This delayed onset is consistent with compensatory reactivation of ERK to offset WEE1 inhibition-induced growth suppression. To address this possibility, we determined whether concurrent ERK inhibition enhances WEE1i growth inhibitory activity. We treated a panel of cell lines with both

WEE1i and the ERK1/2-selective inhibitor SCH772984 (ERKi), which resulted in fewer colonies than treatment with either inhibitor alone (Fig. 5A). BLISS synergy analysis revealed that the combination exhibited synergistic activity in three cell lines (MIA PaCa-2, Pa16C, and Pa02C) and additive activity in three cell lines (Fig. 5, *B* and *C*). Combining low-dose ERK inhibition (IC_{25}–IC_{50}) with WEE1 inhibition also synergistically induced apoptosis in four of four cell lines (Fig. 5, *D* and *E*). We conclude that concurrent inhibition of WEE1 and ERK synergistically induces both growth arrest and apoptosis in PDAC cell lines.

Inhibition of WEE1 + ERK1/2 arrests growth of PDAC organoids

3D patient-derived pancreatic cancer organoids maintained in Matrigel are believed to better model the therapeutic response of PDAC patients than cells grown in 2D culture (58, 59). Therefore, we next evaluated the impact of concurrent WEE1 and ERK inhibition on proliferation of KRAS-mutant PDAC organoid cultures. The combination of inhibitors caused organoids to collapse and shrink more than either inhibitor alone (Figs. 6A and S5, *A* and *B*). Concurrent WEE1 and ERK inhibition caused additive or synergistic effects on viability, depending on doses (Fig. 6, *B* and *C*). Taken together with anchorage-dependent growth assays, we conclude that concurrent ERKi treatment to block compensatory ERK activation can enhance WEE1 inhibition–mediated growth suppression.

Discussion

It is now well appreciated that the effectiveness of pharmacological inhibition of key cancer drivers is offset by the induction of compensatory activities (16, 17, 60, 61). Therefore, identification of treatment-induced compensatory mechanisms can guide the development of combination approaches to better achieve long-term and durable clinical responses. The recent development of direct inhibitors of KRAS (5, 6) has made it even more critical to understand the compensatory activities that can drive resistance to KRAS suppression. In the present study, we applied an activity-dependent chemical proteomics strategy, MIB/MS, to profile the KRAS-dependent kinome in KRAS-mutant PDAC. We identified a diverse spectrum of kinases that were downregulated or upregulated in response to KRAS depletion; many of these had not previously been associated with KRAS effector signaling. We speculated that both groups of kinases may be effective therapeutic targets, with upregulated kinases representing compensatory mechanisms that drive resistance to KRAS suppression. We identified upregulation of DDR1 as one such mechanism and showed that DDR1 inhibition suppressed the growth of KRAS mutant PDAC lines. Conversely, our characterization of one downregulated kinase, WEE1, showed that this DNA damage checkpoint inhibitor can also serve as a therapeutic target. One limitation to MIB/MS data is the inability to distinguish kinase activity changes from kinase expression changes, which requires further validation of any significant change that is identified. Despite this limitation, our study demonstrates the utility of kinome-wide profiling to identify novel strategies for targeting KRAS-mutant PDAC.

Our application of the MIB/MS proteomics screen identified a spectrum of kinases that were downregulated or upregulated upon acute KRAS suppression. We detected a total of 227 kinases in one or more of the six KRAS-mutant PDAC cell lines analyzed. Of these, 125 (55%) were altered in activation and/or expression in one or more lines upon KRAS suppression, underscoring the diverse consequences that aberrant KRAS function confers upon the human kinome. It is likely that even this is a substantial underestimate: the human kinome encodes over 500 protein kinases. Some kinases were not detected here because they are not recognized by any one of the six broad-spectrum kinase inhibitors used in the affinity purification step; others were not detected because of low or lack of expression in pancreatic cancer (62).

Furthermore, although the genetic landscape of PDAC is dominated by the frequent occurrence of alterations in only four genes (*KRAS*, *TP53*, *CDKN2A*, and *SMAD4*), the majority of genetic alterations are found at frequencies of less than 5% (63). Of the 125 KRAS-deregulated kinases, only 28 (22%) were altered across all six KRAS-mutant PDAC lines. Our utilization of additional cell lines for RPPA analysis and follow-up validation further underscored the variability between KRAS-mutant PDAC cell lines. A limitation of using RPPA as a validation tool for our MIB/MS finding is the inherently small (80–150) panel of antibodies that can be included at one time. While more parallelized than a traditional Western blot, many findings from MIB/MS were not able to be directly including in RPPA because of the lack of validated antibody availability. All cell lines used in this study are dependent on mutant KRAS but have varied growth dependency on ERK activity (13). This observed heterogeneity is thus consistent with the genetic heterogeneity of PDAC and highlights the distinct and significant impact that co-occurring mutations may have on KRAS function, and, consequently, on response to specific therapies.

We observed significant overlap of the kinase activity/expression changes caused by acute genetic suppression of KRAS compared with those caused by pharmacological inhibition of ERK. Nine of 13 KRAS-downregulated kinases and four of 15 KRAS-upregulated kinases were also altered upon ERK inhibition. That we observed a dominant role of the ERK MAPK cascade in regulating the KRAS-dependent kinome is consistent with the critical role of this protein kinase cascade in driving KRAS-dependent PDAC growth. Nevertheless, many of the 28 KRAS-regulated kinases are not known to be directly associated with ERK signaling. Only eight (CKIIε, CDK1, CHK1, ERK1, ephrin type-A receptor 2, SRPK2, TRAF and NCIK-interacting protein kinase, and TTK) are listed in a recent compilation of direct or indirect ERK substrates from 14 different phosphoproteomic studies (10). However, it is still possible that some of the other 20 KRAS-regulated kinases are ERK substrates. The compilation includes no studies performed in PDAC. In our ongoing phosphoproteomic analyses of ERK-dependent phosphorylation in PDAC, we have
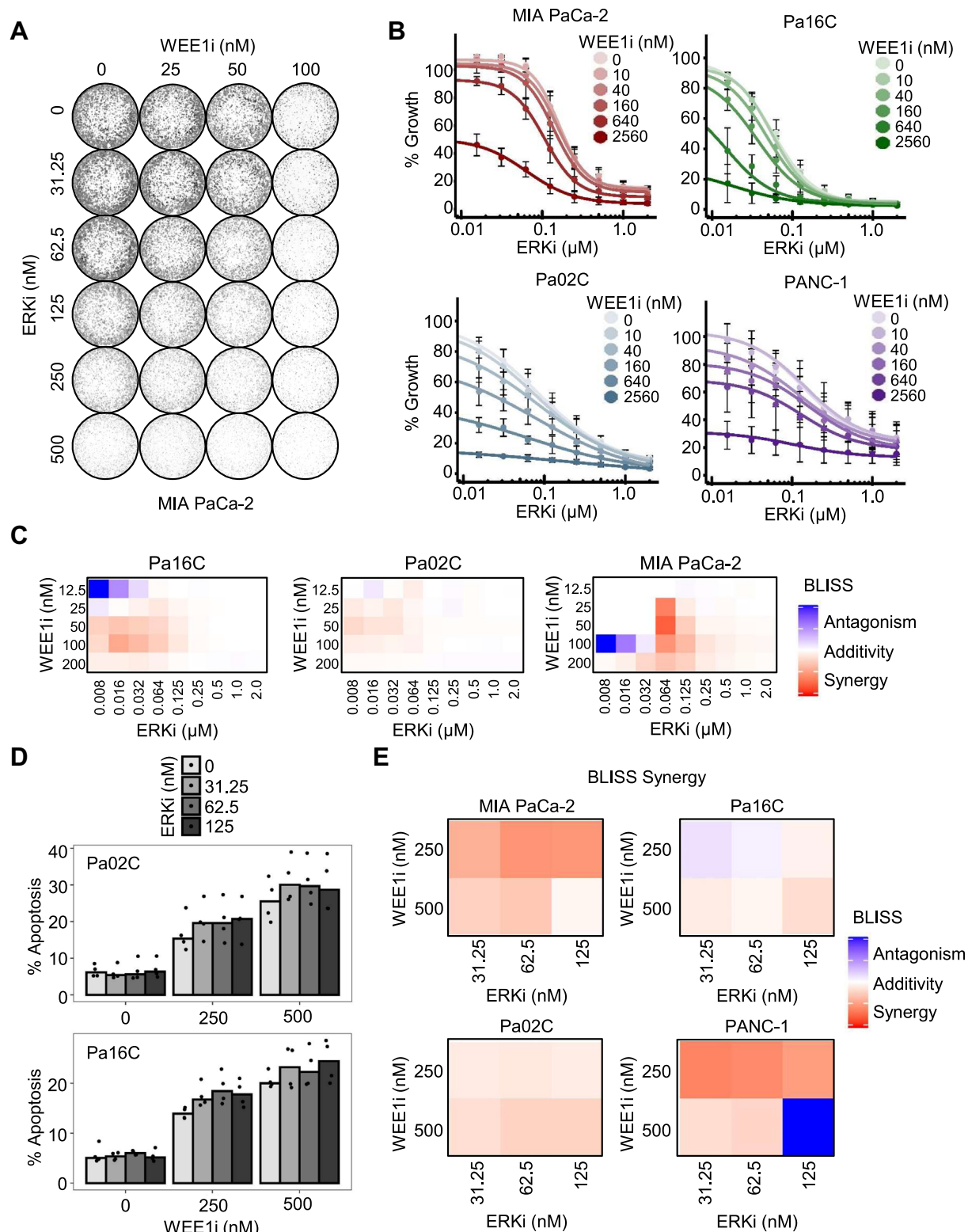
Figure 5. Combined inhibition of WEE1 and ERK induces growth arrest and apoptosis. *A*, PDAC cells were plated at low density, and various concentrations of WEE1i (adavosertib) and/or ERKi (SCH772984) were added to the media. Cells were permitted to grow for 10 days to allow for clonogenic growth. Plates were then stained with crystal violet and imaged (n = 3). *B*, proliferation of PDAC cells following treatment for 5 days with WEE1i (adavosertib) and ERKi (SCH772984) at various concentrations in combination. Cell numbers at endpoint were normalized to vehicle-treated control (100% growth) for each cell line. Curves were fit using a 4-parameter log-logistic function and the drm package in R (n = 4). *C*, BLISS Synergy scores were calculated using the proliferation effect sizes from panel *B*. Scores <1 indicate synergy (*red*), scores = 1 indicate additivity (*white*), and scores >1 indicate antagonism (*blue*) (n = 4). *D*, annexin V–FITC staining followed by flow cytometry in PDAC cell lines after 72 h treatment with WEE1i. Quantification of apoptosis at each dose combination is displayed for the indicated cell lines (n = 4). *E*, BLISS Synergy scores were calculated using the proliferation effect sizes from panel *D*. Scores as for panel *C*, representative heatmaps are shown (n = 4). ERK, extracellular signal–regulated kinase; ERKi, ERK inhibitor; PDAC, pancreatic ductal adenocarcinoma.
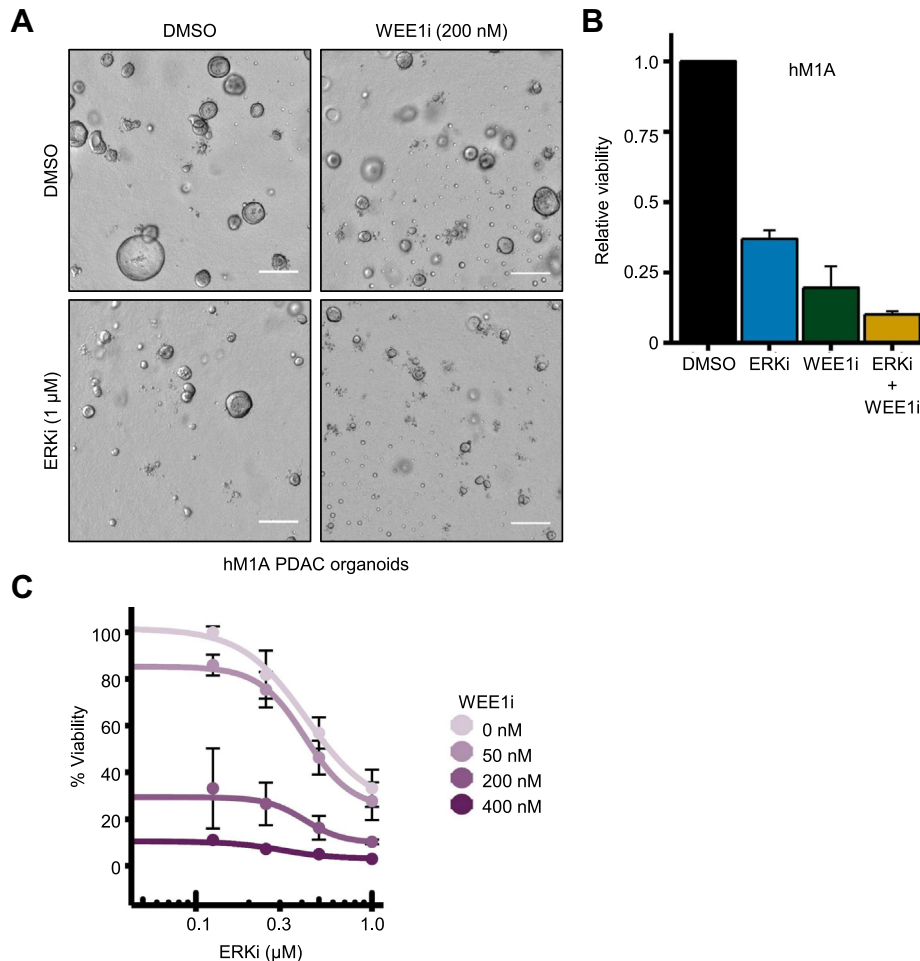
Figure 6. Inhibition of WEE1 + ERK1/2 arrests growth of PDAC organoids. *A*, hM1A PDAC organoids were seeded for 3 days in Matrigel and organoid maintenance factors, followed by treatment for 10 days with ERKi or WEE1i or the combination. Representative images are shown; scale bar is equivalent to 200 μm (n = 4). *B*, quantification of CellTiter-Glo 3D cell viability assay in organoids at single-dose combination from panel *A*. *C*, organoids from (*A*) were quantified using CellTiter-Glo 3D cell viability assay across a range of WEE1i (adavosertib) and ERKi (SCH772984) doses. Percent viability was normalized to DMSO-treated organoids at the assay endpoint. ERK, extracellular signal–regulated kinase; ERKi, ERK inhibitor; DMSO, dimethyl sulfoxide; PDAC, pancreatic ductal adenocarcinoma.

identified numerous potential direct or indirect ERK substrates that have not been identified previously. Finally, none of the 28 kinases identified in the present study are listed in the Gene Set Enrichment Analysis KRAS gene signature, indicating that many of the kinases we detected are altered in activity rather than by gene expression.

Finally, some observed alterations may be indirect rather than associated specifically with KRAS signaling. For example, reduced kinase expression may be a consequence of the incomplete G1 arrest caused by KRAS suppression. NEK2 is undetectable during G1 but accumulates progressively throughout S phase, reaching maximal levels in late G2 phase (64).

Our working hypothesis for this study was that the kinases that are upregulated upon KRAS suppression would be distinct from those typically utilized by KRAS for its transforming activities. Instead, it is now well established that compensatory kinome reprogramming occurs upon pharmacological inhibition of RAF and PI3K signaling (22, 23). We hypothesized that loss of KRAS signaling would similarly induce compensatory kinome reprogramming, such that the upregulated kinases would enable maintenance of the transformed phenotype. Consistent with this possibility was the significant enrichment of upregulated tyrosine kinases, a class that includes many oncogenic kinases (*e.g.*, EGFR, human epidermal growth factor receptor 2, etc.). To evaluate this possibility, we selected two kinases, JAK1 and DDR1, for validation analyses. Since there is evidence that JAK1 can act as a cancer driver in multiple cancer types (65), we were surprised that pharmacological inhibition of JAK1, either alone or together with ERK inhibition, did not negatively impact PDAC growth. This finding emphasizes that the potential therapeutic value of an upregulated or hyperactivated kinase requires functional validation, not simply evidence of increased expression or activity.

In contrast to JAK1, we verified that pharmacological inhibition of DDR1 alone or in combination with an ERKi caused additive or synergistic growth suppression of PDAC cell lines. To date, there has been limited effort in the pursuit of DDR1 as a therapeutic target in PDAC, and there are no clinically tractable DDR1-specific inhibitors. However, the DDR1-selective pharmacological inhibitor 7rh, together with chemotherapy, impaired tumorigenic growth of PDAC cell

lines ([48]). In a complementary study, genetic ablation of *Ddr1* in the KPC (*Kras*[G12D/+]; *Tp53*[R172/+]) mouse model of PDAC impaired metastatic tumor growth ([47]). Finally, a recent kinome profiling screen using a different experimental method than MIB/MS demonstrated upregulation of DDR1 expression in patient-derived PDAC cell lines ([66]). In agreement, we observed that direct pharmacological inhibition of DDR1 with the small molecule inhibitor 7rh suppressed PDAC cell proliferation *in vitro*. Specific cell line responses to the DDR1 inhibitor varied; however, these were not explained by any consistent underlying genetic driver mutations. In addition, we observed synergistic reduction in proliferation when we combined the DDR1 inhibitor with the ERK1/2-selective inhibitor SCH772984, supporting further evaluation of this combinatorial therapeutic strategy. Our identification of DDR1 as a mediator of resistance to KRAS suppression in PDAC is limited by the breadth of genetic heterogeneity available in the panel of cell lines used. Future work should focus on expanding these analyses both to a broader array of cell lines as well as inclusion of 3D organoid PDAC cell systems, which better predict *in vivo* physiology ([58], [59]).

The downregulated kinases were enriched (11 of 13) in kinases that modulate cell cycle progression, particularly processes involved in mitosis. Inhibition of some of these individual kinases is sufficient to impair cancer growth, indicating that KRAS regulates growth through a multitude of mechanisms. For example, PLK1 has been identified as a synthetic lethal interactor with mutant RAS ([67]). We showed previously that pharmacological inhibition of TTK impaired PDAC growth ([68]). In agreement with previous studies ([63], [69]–[71]), we showed here that inhibition of WEE1 suppresses PDAC growth. In addition, we found that concurrent ERK inhibition, to counter the compensatory ERK activation associated with WEE1 inhibition, further enhanced WEE1i growth-inhibitory activity. Strikingly, concurrent WEE1i and ERKi effectively reduced growth of both 2D adherent PDAC cultures as well as 3D organoid cultures. The WEE1i adavosertib is currently being evaluated alone or in combination with other anticancer therapies in 20 active or recruiting clinical trials, including one in pancreatic cancer (NCT02194829, accessed February 22, 2021).

In summary, the MIB/MS chemical proteomics strategy provides a powerful experimental approach to delineate a more complete understanding of the KRAS-dependent kinome, implicating kinases not identified by other methods. We in addition showed that both downregulated and upregulated kinases upon loss of KRAS represent potential therapeutic targets for PDAC treatment. Our findings also further establish mechanisms by which the ERK MAPK effector pathway drives KRAS-dependent PDAC growth, through regulation of multiple distinct regulators of cell cycle progression, particularly mitosis. Finally, that KRAS suppression caused upregulation of a diverse spectrum of functionally distinct kinases underscores the need to develop combination inhibitor therapies to thwart treatment-induced kinome reprogramming, which will result in acquired resistance and

limit the long-term efficacy of mutant-specific KRAS inhibitors.

Experimental procedures

Cell culture

Cell lines were obtained from the American Type Culture Collection (AsPC-1, Panc10.05, SW-1990, MIA PaCa-2, PANC-1, HPAC, and HPAF-II) or were a gift from J. Fleming at MD Anderson Cancer Center (Pa01C, Pa02C, Pa14C, and Pa16C). Cells were maintained in either Dulbecco's minimum essential medium (Gibco; 11995-065; MIA PaCa-2, PANC-1, HPAC, HPAF-II, Pa01C, Pa02C, Pa14C, and Pa16C) or RPMI1640 (Gibco; AsPC-1, Panc 10.05, and SW-1990) supplemented with 10% fetal bovine serum (Sigma–Aldrich) as well as penicillin and streptomycin (Sigma–Aldrich). All cell lines were short-tandem repeat profiled to confirm their identity. All cell lines tested negative for *mycoplasma* contamination.

Antibodies and reagents

SCH772984 was provided by Merck. The following compounds were purchased from Selleckchem: adavosertib (S1525), filgotinib (S7605), ruxolitinib (S5243), and tofacitinib (S2789); or from Sigma–Aldrich: 7rh (SML1832) and MG-132 (M7449). The following antibodies were obtained from Cell Signaling Technology: anti-DDR1 (5583S), anti-PYK2 (3090S), anti-STAT3 (9139S), antiphosphorylated STAT3 Tyr[705] (9145S), anti-WEE1 (13084S), anti-CHK1 (2360S), anti-PLK1 (4513T), anti-ERK (4696S), antiphosphorylated ERK Thr[202]/Tyr[204] (4370S), antiphosphorylated CDC2 Tyr[15] (4539S), antiphosphorylated Histone H3 Ser[10] (53348S); from Sigma–Aldrich: antivinculin (V9131), anti-β-actin (A5441), and anti-KRAS (WH0003845M1); from Invitrogen: antiphosphorylated PYK2 Tyr[402] (44-618G); or from Santa Cruz Biotechnology: anti-CDC2 (sc-54).

RNAi knockdown studies

siRNA experiments were performed with 10 nM siRNA and RNAiMAX Lipofectamine (Invitrogen; 13778150) according to the manufacturer's protocol. siRNAs were obtained from Thermo Fisher: nonspecific siRNA (4390844), siKRAS-1 (4390825-s7939), siKRAS-2 (4390825-s7940), siWEE1-1 (4390824-s21), siWEE1-2 (AM51331-404), siDDR1-1 (4390824-s2298), and siDDR1-2 (4390824-s2230). On day 1, cells were plated at 2×10^5 cells per well of a 6-well plate. On day 0, Lipofectamine was warmed to room temperature and added to Opti-MEM (Gibco; 31985-070) to a final concentration of 20× before low-speed vortex. siRNAs were added to individual tubes of Opti-MEM at 20× concentration. Both Lipofectamine and siRNA tubes were incubated at room temperature separately for 5 min. After incubation, Lipofectamine in Opti-MEM was combined at a 1:1 ratio with individual siRNAs in Opti-MEM. Tubes were carefully inverted five to seven times to mix Lipofectamine and siRNA in Opti-MEM and were subsequently incubated at room temperature for 30 min. Two hundred microliters of the Lipofectamine

with siRNA were added to 1.8 ml of fresh cell culture media per well. Cells were incubated for specified times before collection for immunoblotting, proliferation, clonogenic, cell cycle, or apoptosis assays.

For quantitative RT–PCR experiments, the aforementioned transfection protocol was modified to combine the day 1 and day 0 steps. Cells (2×10^5) were plated in 1.8 ml cell culture medium with the addition of 200 μl of Lipofectamine with respective siRNA on day 0.

MIB–MS

Samples were prepared according to the RNAi knockdown protocol outlined in Experimental procedures section. Following 72 h of RNAi knockdown with either nonspecific siRNA or siKRAS 1, the cell plates were placed on ice and the cells were washed 5× with large volume ice-cold PBS. The final PBS wash was thoroughly aspirated, and MIB/MS lysis buffer (50 mM Hepes [pH 7.5], 0.5% Triton X-100, 150 mM NaCl, 1 mM EDTA, 1 mM EGTA, 10 mM sodium fluoride, 2.5 mM sodium orthovanadate, protease inhibitor cocktail [Roche], 1% phosphatase inhibitor cocktail 2 [Sigma–Aldrich], and 1% of phosphatase inhibitor cocktail 3 [Sigma–Aldrich]) was added to the adherent cells and permitted to incubate on ice for 5 min. Using a rubber cell scraper, cell lysates were transferred from the plates to 1.7 ml microcentrifuge tubes and placed on ice for 10 min. Cell lysates were subsequently sonicated four times for 15 s at 50% power, alternating between samples to allow cooling on ice between pulses. Cell lysates were then centrifuged at top speed (13,200 rpm) for 10 min at 4 °C. Supernatants were clarified using a 0.2 μm filter, transferred into labeled tubes, and stored at –80 °C (∼5 mg protein per experiment). A small portion of lysate was removed for Bradford assay estimation of protein concentration. The lysates were thawed and gravity flowed over multiplexed kinase inhibitor beads (MIBs; Sepharose conjugated to VI-16832, CTx-0294885, PP58, Purvalanol B, UNC8088A, and UNC21474). MIBs were then washed with high salt (1 M NaCl) and low salt (150 mM NaCl + 0.1% SDS) lysis buffers without the inhibitors. The samples were boiled with the elution buffer (100 mM Tris–HCl, 0.5% SDS, and 1% β-mercaptoethanol, pH 6.8) at 100 °C for 5 min to elute the bound kinases from MIBs. The eluted kinases (proteins) were concentrated with Amicon Ultra-4 (cutoff of 10,000) spin columns (Millipore), purified by removing the detergent using methanol/chloroform extraction, and digested by sequencing-grade trypsin (Promega) overnight at 37 °C. Hydrated ethyl acetate extraction was used to remove Triton, and PepClean C18 spin columns (Thermo Fisher Scientific) were used to desalt the digested peptides.

Biological triplicates of the MIB samples were analyzed by LC–MS/MS as we described previously (32). Briefly, each sample was injected onto an EASY-Spray PepMap C18 column (75 mm id 3 25 cm, 2 mm particle size) (Thermo Fisher Scientific) and separated over a method of 2 h. The gradient for separation consisted of 5–32% mobile phase B at a 250 nl/min flow rate, where mobile phase A was 0.1% formic acid in water and mobile phase B consisted of 0.1% formic acid in

acetonitrile. The Thermo QExactive HF was operated in data-dependent mode where the 15 most intense precursors were selected for subsequent higher energy collision dissociation fragmentation (set to 27%).

Raw data files were processed using MaxQuant, version 1.6.3.4, and searched against the reviewed UniProt human database (downloaded January 2019, containing 20,414 sequences) using Andromeda within MaxQuant. Enzyme specificity was set to trypsin, up to two missed cleavage sites were allowed, carbamidomethylation of Cys was set as a fixed modification, and oxidation of Met was set as a variable modification. The mass tolerance for precursor (main search) and product ions was set to 6 and 20 ppm, respectively. Label-free quantification (LFQ) using razor + unique peptides was enabled. A 1% false discovery rate was calculated within MaxQuant and used to filter all data. Only proteins with >1 peptides were used for downstream analyses. Following Max-Quant processing of data and generation of LFQ intensity values, data files were analyzed using R (version 3.5.2). Kinases were excluded if they were not present in >50% of samples or if they contained two or more peptides. For imputation of missing values, a normal distribution was modeled on the nonmissing LFQ intensity values of the kinases containing missing intensity values. Imputed values were drawn randomly from this distribution. Following filtering and imputation, LFQ intensity values were log2 transformed, and the fold change over the median vehicle value was calculated for each kinase. Kinases significantly different between treatments with siNS and siKRAS, or with dimethyl sulfoxide and ERKi, were determined using one-way ANOVA (Benjamini–Hochberg adjusted-p value <0.05). Euclidean distance and average linkage were utilized for unsupervised hierarchical clustering of log2 fold-change values for significant kinases.

Immunoblotting

Plates containing the PDAC cell lines were washed with PBS and lysed with Triton X-100 lysis buffer (25 mM Tris buffer, 100 mM NaCl, 1 mM EDTA, and 1% Triton X-100), supplemented with cOmplete protease inhibitor (Roche) and Phosphatase Inhibitor Cocktail (Sigma–Aldrich). Cells were incubated on ice for 10 min before scraping into a microcentrifuge tube and placed back on ice. Sample tubes were centrifuged for 10 min at 13,200 rpm at 4 °C. The supernatant was collected and used to determine protein concentration using a Bradford Assay (Bio-Rad), and samples were prepared with 4× Laemmli sample buffer (Bio-Rad). Samples were then boiled and stored at –20 °C. About 10% polyacrylamide gels were used to clarify lysates before transferring onto polyvinylidene fluoride membranes (Millipore; IPVH00010) at 90 V for 90 min. Membranes were blocked for 1 h in 5% bovine serum albumin solution diluted in TBST (TBS with 0.05% Tween-20) and washed with TBST. Membranes incubated overnight in primary antibodies diluted in 5% bovine serum albumin solution supplemented with sodium azide. Secondary antibodies used were goat antimouse (Invitrogen; 31432) and goat anti-rabbit (Invitrogen; 31462). Membranes

were washed with TBST before imaging using the ChemiDoc MP Imaging System (Bio-Rad) and ECL reagent.

Quantitative real-time PCR

Cells were grown in 6-well plates, transfected with siRNA as indicated, and harvested. RNA was extracted using the RNeasy Isolation Kit (Qiagen) and converted to cDNA using the High-Capacity cDNA Reverse Transcription Kit (Applied Biosystems). RT–PCR was performed using the TaqMan system (Applied Biosystems) in a 384-well format. 6-Carboxyfluorescein-labeled target primer and endogenous human ACTB control (beta actin) (Thermo Fisher Scientific) were mixed with master mix and template and after 40 cycles were analyzed on an QuantStudio 6 Flex Real-Time PCR System (Applied Biosystems).

Flow cytometry

For apoptosis assays, TACS Annexin V-FITC Kits (BD Biosciences) were utilized to measure apoptosis. The following protocol is closely adapted from the manufacturer's specifications. Prior to trypsinization, floating cells in the spent culture medium were collected. Cells were then trypsinized cells and collected, mixed, and centrifuged at 300*g* for 5 min at room temperature. The cells were washed with PBS and centrifuged at 300*g* for 5 min before incubating the cell pellet in annexin V staining solution (1% annexin V–FITC, propidium iodide solution, in 1× calcium-containing binding buffer) in the dark for 15 min at room temperature. Cell mixture was subsequently diluted 1:5 in binding buffer. For cell cycle analysis, adherent cells were washed with PBS prior to being trypsinized. After trypsinization, cells were centrifuged at 300*g* for 5 min before washing once in PBS. Cells were pelleted and resuspended in 1 ml PBS before adding 9 ml of 70% ethanol drop-wise to each tube with gentle agitation. Cells were permitted to fix for a minimum of 18 h at 4 °C. Fixed cells were then pelleted, washed once in PBS, resuspended in 40 µg/ml propidium iodide (PI), 100 µg/ml RNase A in PBS, and incubated at 37 °C for 3 h.

Apoptosis assays were analyzed using FCS Express. A FSC-A *versus* SSC-A dot plot was used to exclude debris and generate a "cells" gate. "Cells" were plotted in a FITC-A (*x*) *versus* PI-A (*y*) dot plot, and apoptotic cells (FITC+) were analyzed. Cell cycle analyses were performed with FCS Express. After first establishing a "cells" gate, a "singlets" gate was determined using a FSC-A (*x*) *versus* FSC-H (*y*) dot plot. Singlets were then analyzed in a histogram for PI-A content before employing the Multicycle algorithm to analyze cell cycle.

RPPA

Samples were prepared according to the RNAi knockdown protocol outlined in Experimental procedures section. Following 72 h of RNAi-mediated knockdown with nonspecific siRNA, siKRAS-1, or siKRAS-2, plates were washed three times with PBS. Cell lysates were prepared as previously described (27). Coomassie Protein Assay Reagent kit (Thermo

Fisher Scientific) was used to measure protein concentration, following the manufacturer's instructions. Tris–glycine SDS 2× sample buffer (Life Technologies) with 5% β-mercaptoethanol was used to dilute cell lysates to 0.5 mg/ml. Samples were boiled for 8 min and stored at −20 °C until arrayed. An Aushon 2470 automated system (Aushon BioSystems) (72) was used to immobilize cell lysates and the internal controls and print in technical replicates (n = 3) onto nitrocellulose-coated glass slides (Grace Bio-Labs). Sypro Ruby Protein Blot Stain (Molecular Probes) was used to quantify protein concentration in each sample, following the manufacturer's instructions. Reblot Antibody Stripping solution (Chemicon) was used to pretreat the remaining arrays (15 min at room temperature). The arrays were washed with PBS and incubated in Iblock (Tropix) for 5 h before antibody staining (38). Arrays were incubated with 3% H_2O_2, avidin, biotin (DakoCytomation), and an additional serum-free protein block (DakoCytomation) to reduce nonspecific binding of endogenous proteins. Staining was performed using an automated system (DakoCytomation) was used. Each slide was probed for 30 min with one antibody targeting the protein of interest, with 149 antibodies that target proteins involved in signaling networks that regulate cell growth, survival, and metabolism used to probe arrays (Table S3). All antibodies used were validated as described previously (73). Signal amplification was determined by using biotinylated anti-rabbit (Vector Laboratories) or antimouse secondary antibody (DakoCytomation) and a commercially available tyramide-based avidin–biotin amplification system (Catalyzed Signal Amplification System; DakoCytomation). IRDye 680RD streptavidin (LI-COR Biosciences) fluorescent detection system was used. TECAN laser scanner was used to scan Sypro Ruby and antibody-stained slides, and the images were analyzed using commercially available software (MicroVigene, version 5.1.0.0; VigeneTech, Inc) as previously described (74).

Proliferation assays

For 96-well-format growth assays, 10^3 cells per well were plated on day 1 in 200 µl cell culture media. Following overnight incubation, one plate per cell line was isolated on day 0 and quantified by counting calcein acetoxymethyl (AM) positive (500 nM, 20 min)-labeled live cells using the SpectraMax i3x multimode detection platform (Molecular Devices) for the assessment of plating efficiency. Next, we utilized the TECAN 300D dispenser to add inhibitor titrations to the plates. Dose ranges used are indicated in figures and/or figure panels. Dimethyl sulfoxide was kept at or below 0.01% final concentration. Cells were incubated at 37 °C and 5% CO_2 for 5 days. Plates were quantified using calcein AM staining (500 nM, 20 min) followed by counting of positively stained cells using the SpectraMax i3x multimode detection platform. Raw cell numbers were minimally adjusted by cell line depending on the plating efficiency determined on day 0. Next, raw cell counts (positively labeled with calcein AM) were normalized to the untreated wells. One hundred percent growth was assigned to an average of the untreated well cell

counts, all treated wells were calculated relative to this number, and technical replicates were averaged together. Growth curves were constructed by first modeling the raw data with the drc R package (version 3.0-1) and the four-parameter log-logistic function LL.4 (4PL). Next, we isolated the GI_{50} values from the models and drew the growth curves using the ggplot2 package in R (version 3.3.2).

BLISS synergy analysis

First, quantifications of proliferation assays (2D or 3D cultures) were normalized to untreated controls (100% growth). Next, treatment effect sizes were calculated by subtracting the growth percentage (as a decimal) from 1. Values above 1 were removed from BLISS analysis (corresponding to treatments that stimulated cell growth above untreated control). Expected effect sizes for each treatment combination were calculated according to the BLISS algorithm (75). Expected effect size was then divided by observed effect size, and the results were mapped to a color scale (0–1 are shades of red, indicative of "synergy;" 1 is white, indicative of additivity; greater than 1 are shades of blue, indicative of "antagonism") and plotted as a heatmap using the ComplexHeatmap package in R (version 2.4.3).

Proteasome inhibitor studies

Knockdown was performed in the manner described in the Experimental procedures section using either nonspecific siRNA, siKRAS 1, or siKRAS 2. Following incubation with respective siRNA for 68 h, the cell culture medium was replaced with standard cell culture medium supplemented with vehicle or 10 μM MG132. The cells were then incubated at 37 °C for 4 h before using the standard immunoblotting protocol as described in the Experimental procedures section.

Data availability

The MS proteomics data have been deposited to the PRIDE Archive (http://www.ebi.ac.uk/pride/archive/) *via* the PRIDE partner repository with the dataset identifier PXD025819. Data from this study are available in the supporting information.

Author contributions—J. N. D. and C. J. D. conceptualization; J. N. D. methodology; J. N. D. and N. U. R. software; J. N. D., K. R. S., P. S. H., Z. D. K., B. P., R. Y., and R. G. H. validation; J. N. D. formal analysis; J. N. D., J. E. K., K. R. S., P. S. H., D. R. B., Z. D. K., T. S. K. G., E. B., M. P., B. P., R. Y., R. G. H., L. E. H., L. M. G., and C. J. D. investigation; J. N. D. and N. U. R. resources; J. N. D. data curation; J. N. D., K. R. S., P. S. H., and C. J. D. writing–original draft; J. N. D., A. D. C., and C. J. D. writing–review and editing; J. N. D. and C. J. D. visualization; E. F. P., L. E. H., L. M. G., A. D. C., and C. J. D. supervision; J. N. D., T. S. K. G., E. B., M. P., E. F. P., L. E. H., L. M. G., and C. J. D. funding acquisition.

Conflict of interest—C. J. D. is a consultant/advisory board member for Anchiano Therapeutics, Deciphera Pharmaceuticals, Mirati Therapeutics, and Revolution Medicines. C. J. D. has received research funding support from SpringWorks Therapeutics, Mirati Therapeutics, and Deciphera Pharmaceuticals and has consulted for Ribometrix, Sanofi, Jazz Therapeutics, Turning Point Therapeutics, and Eli Lilly. A. D. C. has consulted for Eli Lilly and Mirati Therapeutics. E. F. P. and M. P. are inventors on US government and university assigned patents and patent applications that cover aspects of the technologies discussed such as the reverse phase protein microarrays. As inventors, they are entitled to receive royalties as provided by US Law and George Mason University policy. M. P. and E. F. P. receive royalties from and are consultants of TheraLink Technologies, Inc. E. F. P. is a shareholder of TheraLink Technologies, Inc. and a shareholder and consultant of Perthera, Inc. All other authors no conflicts of interest with the contents of this article.

Abbreviations—The abbreviations used are: AM, acetoxymethyl; cDNA, complementary DNA; DDR1, discoidin domain receptor 1; EGFR, epidermal growth factor receptor; ERK, extracellular signal–regulated kinase; ERKi, ERK inhibitor; JAK, Janus kinase; LFQ, label-free quantification; MAPK, mitogen-activated protein kinase; MEK, mitogen-activated protein kinase/ERK kinase; MEKi, MEK inhibitor; MIB, multiplexed inhibitor bead; mTOR, mammalian target of rapamycin; NCI, National Cancer Institute; PDAC, pancreatic ductal adenocarcinoma; PI, propidium iodide; PLK1, polo-like kinase 1; RPPA, reverse phase protein array; RTK, receptor tyrosine kinase; SHP2, SH2 domain–containing phosphatase-2; SOS1, SOS Ras/Rac guanine nucleotide exchange factor 1; STAT3, signal transducer and activator of transcription 3; TBST, TBS with 0.05% Tween-20.

References

1. Siegel, R. L., Miller, K. D., Fuchs, H. E., and Jemal, A. (2021) Cancer statistics, 2021. *CA Cancer J. Clin.* **71**, 7–33
2. Network, C. G. A. R. (2017) Integrated genomic characterization of pancreatic ductal adenocarcinoma. *Cancer Cell* **32**, 185–203.e113
3. Roth, M. T., Cardin, D. B., and Berlin, J. D. (2020) Recent advances in the treatment of pancreatic cancer. *F1000Res* **9**. F1000 Faculty Rev-131
4. Stalnecker, C. A., and Der, C. J. (2020) RAS, wanted dead or alive: Advances in targeting RAS mutant cancers. *Sci. Signal* **13**, eaay6013

5. Hallin, J., Engstrom, L. D., Hargis, L., Calinisan, A., Aranda, R., Briere, D. M., Sudhakar, N., Bowcut, V., Baer, B. R., Ballard, J. A., Burkard, M. R., Fell, J. B., Fischer, J. P., Vigers, G. P., Xue, Y., *et al*. (2020) The KRAS(G12C) inhibitor MRTX849 provides insight toward therapeutic susceptibility of KRAS-mutant cancers in mouse models and patients. *Cancer Discov.* **10**, 54–71

6. Canon, J., Rex, K., Saiki, A. Y., Mohr, C., Cooke, K., Bagal, D., Gaida, K., Holt, T., Knutson, C. G., Koppada, N., Lanman, B. A., Werner, J., Rapaport, A. S., San Miguel, T., Ortiz, R., *et al*. (2019) The clinical KRAS(G12C) inhibitor AMG 510 drives anti-tumour immunity. *Nature* **575**, 217–223

7. Waters, A. M., and Der, C. J. (2018) Kras: The critical driver and therapeutic target for pancreatic cancer. *Cold Spring Harb. Perspect. Med.* **8**, a031435

8. Papke, B., and Der, C. J. (2017) Drugging RAS: Know the enemy. *Science* **355**, 1158–1163

9. Collisson, E. A., Trejo, C. L., Silva, J. M., Gu, S., Korkola, J. E., Heiser, L. M., Charles, R. P., Rabinovich, B. A., Hann, B., Dankort, D., Spellman, P. T., Phillips, W. A., Gray, J. W., and McMahon, M. (2012) A central role for RAF–>MEK–>ERK signaling in the genesis of pancreatic ductal adenocarcinoma. *Cancer Discov.* **2**, 685–693

10. Unal, E. B., Uhlitz, F., and Bluthgen, N. (2017) A compendium of ERK targets. *FEBS Lett.* **591**, 2607–2615

11. Cargnello, M., and Roux, P. P. (2011) Activation and function of the MAPKs and their substrates, the MAPK-activated protein kinases. *Microbiol. Mol. Biol. Rev.* **75**, 50–83

12. Castellano, E., and Downward, J. (2011) RAS interaction with PI3K: More than just another effector pathway. *Genes Cancer* **2**, 261–274

13. Hayes, T. K., Neel, N. F., Hu, C., Gautam, P., Chenard, M., Long, B., Aziz, M., Kassner, M., Bryant, K. L., Pierobon, M., Marayati, R., Kher, S., George, S. D., Xu, M., Wang-Gillam, A., *et al*. (2016) Long-term ERK inhibition in KRAS-mutant pancreatic cancer is associated with MYC degradation and senescence-like growth suppression. *Cancer Cell* **29**, 75–89

14. Villanueva, J., Vultur, A., Lee, J. T., Somasundaram, R., Fukunaga-Kalabis, M., Cipolla, A. K., Wubbenhorst, B., Xu, X., Gimotty, P. A., Kee, D., Santiago-Walker, A. E., Letrero, R., D'Andrea, K., Pushparajan, A., Hayden, J. E., *et al*. (2010) Acquired resistance to BRAF inhibitors mediated by a RAF kinase switch in melanoma can be overcome by cotargeting MEK and IGF-1R/PI3K. *Cancer Cell* **18**, 683–695

15. Furuse, J., and Nagashima, F. (2017) Emerging protein kinase inhibitors for treating pancreatic cancer. *Expert Opin. Emerg. Drugs* **22**, 77–86

16. Trusolino, L., and Bertotti, A. (2012) Compensatory pathways in oncogenic kinase signaling and resistance to targeted therapies: Six degrees of separation. *Cancer Discov.* **2**, 876–880

17. Murray, B. W., and Miller, N. (2015) Durability of kinase-directed therapies–A network perspective on response and resistance. *Mol. Cancer Ther.* **14**, 1975–1984

18. Terrell, E. M., and Morrison, D. K. (2019) Ras-mediated activation of the Raf family kinases. *Cold Spring Harb. Perspect. Med.* **9**, a033746

19. Unni, A. M., Lockwood, W. W., Zejnullahu, K., Lee-Lin, S. Q., and Varmus, H. (2015) Evidence that synthetic lethality underlies the mutual exclusivity of oncogenic KRAS and EGFR mutations in lung adenocarcinoma. *Elife* **4**, e06907

20. Unni, A. M., Harbourne, B., Oh, M. H., Wild, S., Ferrarone, J. R., Lockwood, W. W., and Varmus, H. (2018) Hyperactivation of ERK by multiple mechanisms is toxic to RTK-RAS mutation-driven lung adenocarcinoma cells. *Elife* **7**, e33718

21. Ambrogio, C., Barbacid, M., and Santamaria, D. (2017) *In vivo* oncogenic conflict triggered by co-existing KRAS and EGFR activating mutations in lung adenocarcinoma. *Oncogene* **36**, 2309–2318

22. Lake, D., Correa, S. A., and Muller, J. (2016) Negative feedback regulation of the ERK1/2 MAPK pathway. *Cell Mol. Life Sci.* **73**, 4397–4413

23. Chandarlapaty, S. (2012) Negative feedback and adaptive resistance to the targeted therapy of cancer. *Cancer Discov.* **2**, 311–319

24. Wood, K. C. (2015) Mapping the pathways of resistance to targeted therapies. *Cancer Res.* **75**, 4247–4251

25. Lou, K., Steri, V., Ge, A. Y., Hwang, Y. C., Yogodzinski, C. H., Shkedi, A. R., Choi, A. L. M., Mitchell, D. C., Swaney, D. L., Hann, B., Gordan, J. D.,

Shokat, K. M., and Gilbert, L. A. (2019) KRAS(G12C) inhibition produces a driver-limited state revealing collateral dependencies. *Sci. Signal* **12**, eaaw9450

26. Martz, C. A., Ottina, K. A., Singleton, K. R., Jasper, J. S., Wardell, S. E., Peraza-Penton, A., Anderson, G. R., Winter, P. S., Wang, T., Alley, H. M., Kwong, L. N., Cooper, Z. A., Tetzlaff, M., Chen, P. L., Rathmell, J. C., *et al*. (2014) Systematic identification of signaling pathways with potential to confer anticancer drug resistance. *Sci. Signal* **7**, ra121

27. Ozkan-Dagliyan, I., Diehl, J. N., George, S. D., Schaefer, A., Papke, B., Klotz-Noack, K., Waters, A. M., Goodwin, C. M., Gautam, P., Pierobon, M., Peng, S., Gilbert, T. S. K., Lin, K. H., Dagliyan, O., Wennerberg, K., *et al*. (2020) Low-dose vertical inhibition of the RAF-MEK-ERK cascade causes apoptotic death of KRAS mutant cancers. *Cell Rep.* **31**, 107764

28. Bantscheff, M., Hopf, C., Kruse, U., and Drewes, G. (2007) Proteomics-based strategies in kinase drug discovery. *Ernst. Schering Found. Symp. Proc.*, 1–28

29. Duncan, J. S., Whittle, M. C., Nakamura, K., Abell, A. N., Midland, A. A., Zawistowski, J. S., Johnson, N. L., Granger, D. A., Jordan, N. V., Darr, D. B., Usary, J., Kuan, P. F., Smalley, D. M., Major, B., He, X., *et al*. (2012) Dynamic reprogramming of the kinome in response to targeted MEK inhibition in triple-negative breast cancer. *Cell* **149**, 307–321

30. Krulikas, L. J., McDonald, I. M., Lee, B., Okumu, D. O., East, M. P., Gilbert, T. S. K., Herring, L. E., Golitz, B. T., Wells, C. I., Axtman, A. D., Zuercher, W. J., Willson, T. M., Kireev, D., Yeh, J. J., Johnson, G. L., *et al*. (2018) Application of integrated drug screening/kinome analysis to identify inhibitors of gemcitabine-resistant pancreatic cancer cell growth. *SLAS Discov.* **23**, 850–861

31. Cann, M. L., Herring, L. E., Haar, L. L., Gilbert, T. S. K., Goldfarb, D., Richards, K. L., Graves, L. M., and Lawrence, D. S. (2019) Dasatinib is preferentially active in the activated B-cell subtype of diffuse large B-cell lymphoma. *J. Proteome Res.* **18**, 522–534

32. Vaseva, A. V., Blake, D. R., Gilbert, T. S. K., Ng, S., Hostetter, G., Azam, S. H., Ozkan-Dagliyan, I., Gautam, P., Bryant, K. L., Pearce, K. H., Herring, L. E., Han, H., Graves, L. M., Witkiewicz, A. K., Knudsen, E. S., *et al*. (2018) KRAS suppression-induced degradation of MYC is antagonized by a MEK5-ERK5 compensatory mechanism. *Cancer Cell* **34**, 807–822.e807

33. Jones, S., Zhang, X., Parsons, D. W., Lin, J. C., Leary, R. J., Angenendt, P., Mankoo, P., Carter, H., Kamiyama, H., Jimeno, A., Hong, S. M., Fu, B., Lin, M. T., Calhoun, E. S., Kamiyama, M., *et al*. (2008) Core signaling pathways in human pancreatic cancers revealed by global genomic analyses. *Science* **321**, 1801–1806

34. Biankin, A. V., Waddell, N., Kassahn, K. S., Gingras, M. C., Muthuswamy, L. B., Johns, A. L., Miller, D. K., Wilson, P. J., Patch, A. M., Wu, J., Chang, D. K., Cowley, M. J., Gardiner, B. B., Song, S., Harliwong, I., *et al*. (2012) Pancreatic cancer genomes reveal aberrations in axon guidance pathway genes. *Nature* **491**, 399–405

35. Waddell, N., Pajic, M., Patch, A. M., Chang, D. K., Kassahn, K. S., Bailey, P., Johns, A. L., Miller, D., Nones, K., Quek, K., Quinn, M. C., Robertson, A. J., Fadlullah, M. Z., Bruxner, T. J., Christ, A. N., *et al*. (2015) Whole genomes redefine the mutational landscape of pancreatic cancer. *Nature* **518**, 495–501

36. Witkiewicz, A. K., McMillan, E. A., Balaji, U., Baek, G., Lin, W. C., Mansour, J., Mollaee, M., Wagner, K. U., Koduru, P., Yopp, A., Choti, M. A., Yeo, C. J., McCue, P., White, M. A., and Knudsen, E. S. (2015) Whole-exome sequencing of pancreatic cancer defines genetic diversity and therapeutic targets. *Nat. Commun.* **6**, 6744

37. Cancer Genome Atlas Research Network (2017) Integrated genomic characterization of pancreatic ductal adenocarcinoma. *Cancer Cell* **32**, 185–203.e113

38. Baldelli, E., Calvert, V., Hodge, A., VanMeter, A., Petricoin, E. F., 3rd, and Pierobon, M. (2017) Reverse phase protein microarrays. *Methods Mol. Biol.* **1606**, 149–169

39. Singh, A., Greninger, P., Rhodes, D., Koopman, L., Violette, S., Bardeesy, N., and Settleman, J. (2009) A gene expression signature associated with "K-Ras addiction" reveals regulators of EMT and tumor cell survival. *Cancer Cell* **15**, 489–500

40. Morris, E. J., Jha, S., Restaino, C. R., Dayananth, P., Zhu, H., Cooper, A., Carr, D., Deng, Y., Jin, W., Black, S., Long, B., Liu, J., Dinunzio, E.,

Windsor, W., Zhang, R., *et al.* (2013) Discovery of a novel ERK inhibitor with activity in models of acquired resistance to BRAF and MEK inhibitors. *Cancer Discov.* **3**, 742–750

41. Nagathihalli, N. S., Castellanos, J. A., Lamichhane, P., Messaggio, F., Shi, C., Dai, X., Rai, P., Chen, X., VanSaun, M. N., and Merchant, N. B. (2018) Inverse correlation of STAT3 and MEK signaling mediates resistance to RAS pathway inhibition in pancreatic cancer. *Cancer Res.* **78**, 6235–6246

42. Corcoran, R. B., Contino, G., Deshpande, V., Tzatsos, A., Conrad, C., Benes, C. H., Levy, D. E., Settleman, J., Engelman, J. A., and Bardeesy, N. (2011) STAT3 plays a critical role in KRAS-induced pancreatic tumorigenesis. *Cancer Res.* **71**, 5020–5029

43. Huang, G., Yan, H., Ye, S., Tong, C., and Ying, Q. L. (2014) STAT3 phosphorylation at tyrosine 705 and serine 727 differentially regulates mouse ESC fates. *Stem Cells* **32**, 1149–1160

44. Decker, T., and Kovarik, P. (2000) Serine phosphorylation of STATs. *Oncogene* **19**, 2628–2637

45. Jegatheeswaran, J., Turk, M., and Pope, J. E. (2019) Comparison of Janus kinase inhibitors in the treatment of rheumatoid arthritis: A systemic literature review. *Immunotherapy* **11**, 737–754

46. Leitinger, B. (2014) Discoidin domain receptor functions in physiological and pathological conditions. *Int. Rev. Cell Mol. Biol.* **310**, 39–87

47. Ruggeri, J. M., Franco-Barraza, J., Sohail, A., Zhang, Y., Long, D., Pasca di Magliano, M., Cukierman, E., Fridman, R., and Crawford, H. C. (2020) Discoidin domain receptor 1 (DDR1) is necessary for tissue homeostasis in pancreatic injury and pathogenesis of pancreatic ductal adenocarcinoma. *Am. J. Pathol.* **190**, 1735–1751

48. Aguilera, K. Y., Huang, H., Du, W., Hagopian, M. M., Wang, Z., Hinz, S., Hwang, T. H., Wang, H., Fleming, J. B., Castrillon, D. H., Ren, X., Ding, K., and Brekken, R. A. (2017) Inhibition of discoidin domain receptor 1 reduces collagen-mediated tumorigenicity in pancreatic ductal adenocarcinoma. *Mol. Cancer Ther.* **16**, 2473–2485

49. Gao, M., Duan, L., Luo, J., Zhang, L., Lu, X., Zhang, Y., Zhang, Z., Tu, Z., Xu, Y., Ren, X., and Ding, K. (2013) Discovery and optimization of 3-(2-(Pyrazolo[1,5-a]pyrimidin-6-yl)ethynyl)benzamides as novel selective and orally bioavailable discoidin domain receptor 1 (DDR1) inhibitors. *J. Med. Chem.* **56**, 3281–3295

50. VanArsdale, T., Boshoff, C., Arndt, K. T., and Abraham, R. T. (2015) Molecular pathways: Targeting the cyclin D-CDK4/6 Axis for cancer treatment. *Clin. Cancer Res.* **21**, 2905–2910

51. Ludovini, V., Ricciuti, B., Tofanetti, F. R., Mencaroni, C., Giannarelli, D., Sidoni, A., Reda, M. S., Siggillino, A., Baglivo, S., Crino, L., Bellezza, G., Chiari, R., and Metro, G. (2018) KRAS mutation and DNA repair and synthesis genes in non-small-cell lung cancer. *Mol. Clin. Oncol.* **9**, 689–696

52. Lanman, B. A., Allen, J. R., Allen, J. G., Amegadzie, A. K., Ashton, K. S., Booker, S. K., Chen, J. J., Chen, N., Frohn, M. J., Goodman, G., Kopecky, D. J., Liu, L., Lopez, P., Low, J. D., Ma, V., *et al.* (2020) Discovery of a covalent inhibitor of KRAS(G12C) (AMG 510) for the treatment of solid tumors. *J. Med. Chem.* **63**, 52–65

53. Grabocka, E., Pylayeva-Gupta, Y., Jones, M. J., Lubkov, V., Yemanaberhan, E., Taylor, L., Jeng, H. H., and Bar-Sagi, D. (2014) Wild-type H- and N-Ras promote mutant K-Ras-driven tumorigenesis by modulating the DNA damage response. *Cancer Cell* **25**, 243–256

54. Cuneo, K. C., Morgan, M. A., Sahai, V., Schipper, M. J., Parsels, L. A., Parsels, J. D., Devasia, T., Al-Hawaray, M., Cho, C. S., Nathan, H., Maybaum, J., Zalupski, M. M., and Lawrence, T. S. (2019) Dose escalation trial of the Wee1 inhibitor adavosertib (AZD1775) in combination with gemcitabine and radiation for patients with locally advanced pancreatic cancer. *J. Clin. Oncol.* **37**, 2643–2650

55. Chang, Q., Chandrashekhar, M., Ketela, T., Fedyshyn, Y., Moffat, J., and Hedley, D. (2016) Cytokinetic effects of Wee1 disruption in pancreatic cancer. *Cell Cycle* **15**, 593–604

56. Dai, Y., Chen, S., Pei, X. Y., Almenara, J. A., Kramer, L. B., Venditti, C. A., Dent, P., and Grant, S. (2008) Interruption of the Ras/MEK/ERK signaling cascade enhances Chk1 inhibitor-induced DNA damage *in vitro* and *in vivo* in human multiple myeloma cells. *Blood* **112**, 2439–2449

57. Lee, H. J., Cao, Y., Pham, V., Blackwood, E., Wilson, C., Evangelista, M., Klijn, C., Stokoe, D., and Settleman, J. (2017) Ras-MEK signaling mediates a critical Chk1-dependent DNA damage response in cancer cells. *Mol. Cancer Ther.* **16**, 694–704

58. Boj, S. F., Hwang, C. I., Baker, L. A., Chio, , II, Engle, D. D., Corbo, V., Jager, M., Ponz-Sarvise, M., Tiriac, H., Spector, M. S., Gracanin, A., Oni, T., Yu, K. H., van Boxtel, R., Huch, M., *et al.* (2015) Organoid models of human and mouse ductal pancreatic cancer. *Cell* **160**, 324–338

59. Tiriac, H., Belleau, P., Engle, D. D., Plenker, D., Deschenes, A., Somerville, T. D. D., Froeling, F. E. M., Burkhart, R. A., Denroche, R. E., Jang, G. H., Miyabayashi, K., Young, C. M., Patel, H., Ma, M., LaComb, J. F., *et al.* (2018) Organoid profiling identifies common responders to chemotherapy in pancreatic cancer. *Cancer Discov.* **8**, 1112–1129

60. Santana-Codina, N., Chandhoke, A. S., Yu, Q., Malachowska, B., Kuljanin, M., Gikandi, A., Stanczak, M., Gableske, S., Jedrychowski, M. P., Scott, D. A., Aguirre, A. J., Fendler, W., Gray, N. S., and Mancias, J. D. (2020) Defining and targeting adaptations to oncogenic KRAS(G12C) inhibition using quantitative temporal proteomics. *Cell Rep.* **30**, 4584–4599.e4584

61. Muzumdar, M. D., Chen, P. Y., Dorans, K. J., Chung, K. M., Bhutkar, A., Hong, E., Noll, E. M., Sprick, M. R., Trumpp, A., and Jacks, T. (2017) Survival of pancreatic cancer cells lacking KRAS function. *Nat. Commun.* **8**, 1090

62. Collins, K. A. L., Stuhlmiller, T. J., Zawistowski, J. S., East, M. P., Pham, T. T., Hall, C. R., Goulet, D. R., Bevill, S. M., Angus, S. P., Velarde, S. H., Sciaky, N., Oprea, T. I., Graves, L. M., Johnson, G. L., and Gomez, S. M. (2018) Proteomic analysis defines kinase taxonomies specific for subtypes of breast cancer. *Oncotarget* **9**, 15480–15497

63. Dreyer, S. B., Chang, D. K., Bailey, P., and Biankin, A. V. (2017) Pancreatic cancer genomes: Implications for clinical management and therapeutic development. *Clin. Cancer Res.* **23**, 1638–1646

64. Fang, Y., and Zhang, X. (2016) Targeting NEK2 as a promising therapeutic approach for cancer treatment. *Cell Cycle* **15**, 895–907

65. Brooks, A. J., and Putoczki, T. (2020) JAK-STAT signalling pathway in cancer. *Cancers (Basel)* **12**, 1971

66. Creeden, J. F., Alganem, K., Imami, A. S., Brunicardi, F. C., Liu, S. H., Shukla, R., Tomar, T., Naji, F., and McCullumsmith, R. E. (2020) Kinome array profiling of patient-derived pancreatic ductal adenocarcinoma identifies differentially active protein tyrosine kinases. *Int. J. Mol. Sci.* **21**, 8679

67. Aguirre, A. J., and Hahn, W. C. (2018) Synthetic lethal vulnerabilities in KRAS-mutant cancers. *Cold Spring Harb. Perspect. Med.* **8**, a031518

68. Stratford, J. K., Yan, F., Hill, R. A., Major, M. B., Graves, L. M., Der, C. J., and Yeh, J. J. (2017) Genetic and pharmacological inhibition of TTK impairs pancreatic cancer cell line growth by inducing lethal chromosomal instability. *PLoS One* **12**, e0174863

69. Dreyer, S. B., Upstill-Goddard, R., Paulus-Hock, V., Paris, C., Lampraki, E. M., Dray, E., Serrels, B., Caligiuri, G., Rebus, S., Plenker, D., Galluzzo, Z., Brunton, H., Cunningham, R., Tesson, M., Nourse, C., *et al.* (2021) Targeting DNA damage response and replication stress in pancreatic cancer. *Gastroenterology* **160**, 362–377.e313

70. Weisberg, E., Nonami, A., Chen, Z., Liu, F., Zhang, J., Sattler, M., Nelson, E., Cowens, K., Christie, A. L., Mitsiades, C., Wong, K. K., Liu, Q., Gray, N., and Griffin, J. D. (2015) Identification of Wee1 as a novel therapeutic target for mutant RAS-driven acute leukemia and other malignancies. *Leukemia* **29**, 27–37

71. Hai, J., Liu, S., Bufe, L., Do, K., Chen, T., Wang, X., Ng, C., Li, S., Tsao, M. S., Shapiro, G. I., and Wong, K. K. (2017) Synergy of WEE1 and mTOR inhibition in mutant KRAS-driven lung cancers. *Clin. Cancer Res.* **23**, 6993–7005

72. Pierobon, M., Ramos, C., Wong, S., Hodge, K. A., Aldrich, J., Byron, S., Anthony, S. P., Robert, N. J., Northfelt, D. W., Jahanzeb, M., Vocila, L., Wulfkuhle, J., Gambara, G., Gallagher, R. I., Dunetz, B., *et al.* (2017) Enrichment of PI3K-AKT-mTOR pathway activation in hepatic metastases from breast cancer. *Clin. Cancer Res.* **23**, 4919–4928

73. Signore, M., and Reeder, K. A. (2012) Antibody validation by Western blotting. *Methods Mol. Biol.* **823**, 139–155

74. Baldelli, E., Haura, E. B., Crino, L., Cress, D. W., Ludovini, V., Schabath, M. B., Liotta, L. A., Petricoin, E. F., and Pierobon, M. (2015) Impact of upfront cellular enrichment by laser capture microdissection on protein and phosphoprotein drug target signaling activation measurements in human lung cancer: Implications for personalized medicine. *Proteomics Clin. Appl.* **9**, 928–937

75. Foucquier, J., and Guedj, M. (2015) Analysis of drug combinations: Current methodological landscape. *Pharmacol. Res. Perspect.* **3**, e00149

76. Ashburner, M., Ball, C. A., Blake, J. A., Botstein, D., Butler, H., Cherry, J. M., Davis, A. P., Dolinski, K., Dwight, S. S., Eppig, J. T., Harris, M. A., Hill, D. P., Issel-Tarver, L., Kasarskis, A., Lewis, S., *et al.* (2000) Gene ontology: tool for the unification of biology. The Gene Ontology Consortium. *Nat. Genet.* **25**, 25–29

77. Gene Ontology, C. (2021) The gene Ontology resource: Enriching a GOld mine. *Nucleic Acids Res.* **49**, D325–D334

ASBMB